Understanding the Role of Contrails and Contrail Cirrus in Climate Change: A Global Perspective

Dharmendra Kumar Singh, Swarnali Sanyal, Donald J. Wuebbles

Department of Atmospheric Sciences, University of Illinois Urbana-Champaign, Illinois, USA
Urbana, IL 61802

Correspondence to: Dharmendra Kumar Singh (dksingh8@illinois.edu)

Abstract

Globally emissions from aviation affect the Earth's climate via a complex set of processes. Contrail cirrus and carbon dioxide emissions are the largest factors from aviation in the radiative forcing on climate. Although contrail cirrus enhances the impact of natural clouds on the climate, there are still unresolved questions concerning their characteristics and life cycle. Despite extensive research in studying contrails, significant uncertainties persist. Contrail cirrus encompasses linear contrails and the associated cirrus clouds; these are characterized by ice particle properties, e.g., size, concentration, extinction, ice water content, optical depth, geometrical depth, and cloud coverage. The climate impact of contrails may intensify due to projected increases in air traffic. The radiative forcing from global contrail cirrus has the potential to triple and could reach as much as 160 mW m^{-2} by 2050. This projection is based on anticipated growth in air traffic and a potential shift to higher altitudes. The future climate impact of contrail cirrus is influenced by factors like the magnitude and geographical spread in air traffic, advancements in fuel efficiency, the effects from use of alternative fuels, and the effects of the changing climate on the background atmosphere. This study reviews the microphysical processes affecting contrail formation and the aging of contrails and contrail-cirrus. Furthermore, the study explores global observational datasets for contrails, current analyses, and future projections and will aid in evaluating the effectiveness and trade-offs associated with various mitigation strategies. The research highlights gaps in knowledge and uncertainties while outlining research priorities for the future.

Keywords: Aviation, contrails, contrail cirrus, radiative forcing, climate model, climate change

1 Introduction

The increase in the atmospheric carbon dioxide (CO_2) concentration has had the most substantial impact on human-induced climate change over recent decades (IPCC 2021). Emissions from aviation are a minor but significant contributor to these changes in climate, especially because of emissions of CO_2 and the effects of contrail formation from emitted water vapor (H_2O). Aviation expansion is outpacing economic growth, with projections indicating that over the next two decades, the demand for aviation could grow to about 3 times its present level (Wuebbles et al., 2007), with the International Civil Aviation Organization having previously projected a 4.3% annual growth to 2050 (ICAO 2012). Recent analyses by Boeing and Airbus suggest slightly lower rates of increase of 3.6-3.8% (Boeing 2022; Airbus 2023). These analyses suggest that aviation could become an even more important contributor to climate change in the future. Taking both CO_2 and non-CO_2 effects into account, The global aviation industry comprises about 3.5-4% of the current human-made (anthropogenic) activities forcing on climate (Lee et al., 2020; Klöwer et al., 2021; Grewe et al., 2021).

Contrails and resulting contrail clouds formation is one of the most significant radiative forcing contributors from the aviation sector. (Lee et al., 2009, 2021). However, considerable ambiguities persist, stemming from various origins, such as our incomplete understanding of cirrus cloud characteristics, their geographical distribution, and their life span. (Kärcher 2018; Burkhardt et al., 2018; Schumann and Heymsfield 2017). With current aircraft largely burning fossil fuel, CO_2 emissions are the other major forcing. Additionally, NO_x (oxides of nitrogen) emission also has a notable impact through the production of tropospheric ozone, but this is partially counteracted by chemical feedback effects on concentrations of atmospheric methane (CH_4). Fig. 1 (Lee et al., 2021) provides the most current assessment of the climate-forcing effects resulting from different aviation emissions on a global scale, spanning from 1940 to 2018; these effects are shown in terms of radiative forcing (RF) and effective radiative forcing (ERF). Radiative forcing in the context of contrails is due to the net radiative energy flux at the top of the atmosphere (TOA) caused by the presence of contrails in the atmosphere (Fuglestvedt et al., 2010). A positive radiative forcing (RF) signifies an increase in atmospheric warming, as depicted by the red bars in Figure 1. ERF, on the other hand, adjusts the RF by accounting for rapid responses occurring within the Earth's climate system.

In the scientific literature, contrail cirrus is defined as encompassing both linear contrails and the resulting formation of cirrus clouds. Figure 2 provides an overview of aviation exhaust plume emissions and factors influencing contrail formation. The characteristics of contrail cirrus include average ice particle sizes and concentrations, extinction, ice water content, optical depth, geometrical depth, and contrail coverage. Integral contrail properties involve parameters such as contrail cirrus volume, total number of ice particles, overall ice water content, and total extinction (area integral of extinction) per contrail length.

Many global climate chemistry models used to study the physics and chemistry affecting the Earth's climate system typically do not incorporate the impacts Models that do account for contrails estimate contrail cirrus coverage based on simplified treatments of contrail aging and spreading mechanisms in ice-supersaturated regions (ISSRs) (Burkhardt et al., 2010; Burkhardt and Kärcher 2011; Bock and Burkhardt 2016; Bier and Burkhardt 2022). The generation of persistent contrails depends on coming across ice-supersaturated conditions along a flight path, and these conditions show variability in both space and time within the troposphere and tropopause region (Irvine et al., 2013). Estimating the RF from contrail cirrus requires knowledge of complex

86   microphysical processes, radiative transfer, and the interaction of contrails with background
87   cloudiness (Burkhardt et al., 2010).

88
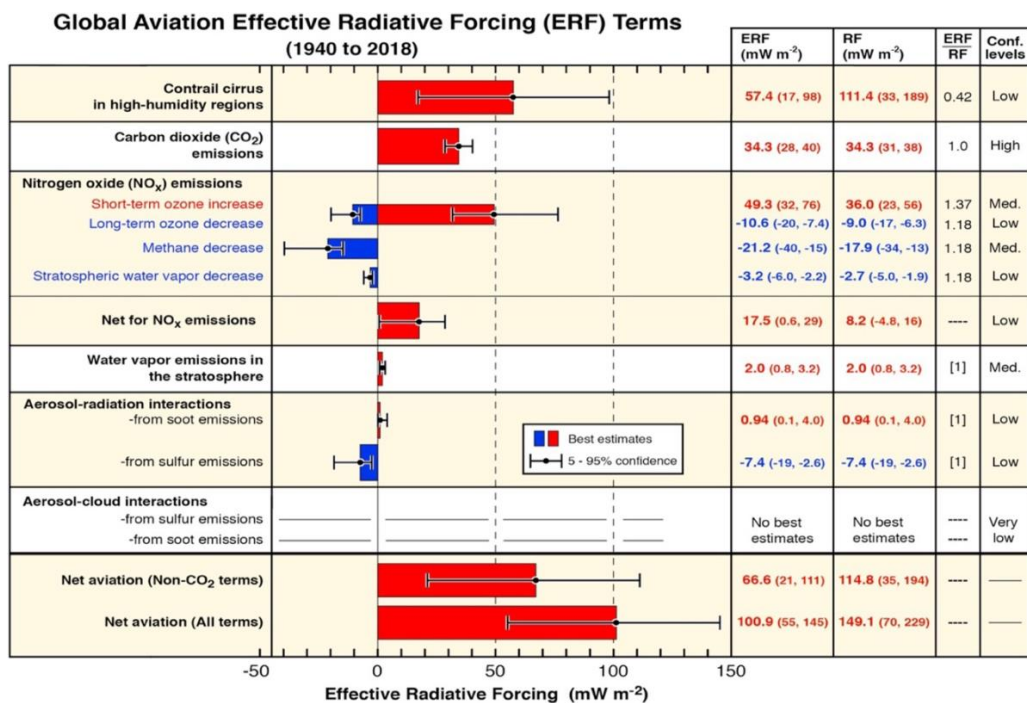
89   **Figure 1.** Current best evaluation of the climate forcing between 1940 and 2018 from commercial
90   aviation for different types of emissions. ERF accounts for short-term feedback in the climate
91   system not accounted for in the traditional RF evaluation. Figure adapted with permission from
92   Lee et al. (2021). (The license is provided by Elsevier and the Copyright Clearance Center; License
93   Number 5682580629967)

94
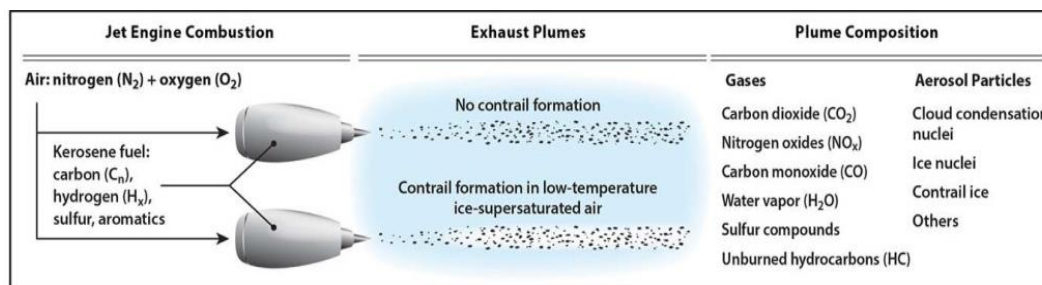
95

96   **Figure 2.** Schematic overview of exhaust plumes (contrail formation in low temperature) and their
97   composition. Figure adapted with permission from Lee et al. (2021). (The license is provided by
98   Elsevier and the Copyright Clearance Center; License Number 5682580629967)

99

100 The aim of this review article is to provide a comprehensive overview of our understanding of
101 contrails, encompassing their formation, progression, and the consequent repercussions on Earth's
102 climate system. In the process, the microphysical processes underlying contrail formation are
103 explored along with their representation in the simulation of contrails in current climate-chemistry
104 models of the global atmosphere. Furthermore, we address the uncertainties surrounding this topic
105 and identify areas requiring further research in the future.

106 **2 Microphysics of Contrail Formation, Aging, And Transition to Contrail Cirrus**

107 Microphysical processes play a pivotal role in the formation of contrails and their evolution in the
108 atmosphere. This section is aimed at discussing these processes, their effects on the lifetime of
109 contrails, and the possible transition of contrails to contrail cirrus in the upper troposphere.

110 **2.1 The Physics of Contrail Formation and Ageing**

111 The fundamental principles for determining the formation of contrails were independently
112 developed by E. Schmidt in 1941 and H. Appleman in 1953. Contrails appear when the hot and
113 moist exhaust from aircraft quickly mixes with the cold and humid surrounding air, causing the
114 humidity in the exhaust gases to exceed the saturation point for liquid water (Appleman 1953;
115 Schmidt 1941; Schumann 1996). A schematic representation of the Schmidt-Appleman criterion
116 for contrail formation is shown in Figure 3. In this diagram, the two solid curves depict saturation
117 levels concerning liquid water (upper curve) and ice (lower curve). The phase trajectory of the
118 mixture, consisting of exhaust gases and ambient air, follows a straight line from the upper right
119 to the lower left in the e-T diagram, where 'e' represents the partial pressure of water vapor in the
120 mixture, and 'T' represents its absolute temperature (as denoted by the dashed lines). The path that
121 lines up with the water saturation curve (dotted) specifies the highest temperatures at which
122 contrail formation can take place. When the trajectory terminates in an ice-supersaturated state,
123 the persisting contrails have the potential to disperse and transform into contrail cirrus.

124 In cases where the conditions do not meet the criteria, the contrail formed will have a brief lifespan,
125 lasting only a few minutes. The mixing process is presumed to occur isobarically, resulting in a
126 straight-line mixing (phase) trajectory on an e-T diagram. The Schmidt–Appleman criterion
127 (SAC), which is primarily based on thermodynamics, establishes the threshold temperature for
128 contrail formation. This threshold is determined by several factors, such as ambient air pressure,
129 humidity, the amount of water and heat released by the aircraft per unit of fuel, and the overall
130 efficiency of the aircraft engine's propulsion system. (Jensen et al., 1998; Schumann, 1996).
131 Accurate assessments of contrails necessitate precise data on ambient meteorological conditions.
132 The persistence of contrails is contingent on meeting a specific humidity threshold, as defined
133 below.

134 The persistence of contrails hinges on the atmospheric specific humidity. Temperature and vertical
135 motions within the atmosphere play key roles in determining relative humidity. Additionally, the
136 optical characteristics and lifespan of contrails are significant dynamics of contrail formation and
137 are influenced by various meteorological factors, especially turbulence, vertical motions, wind
138 shear, and the presence of ambient cirrus clouds. Furthermore, these factors are influenced by the
139 soot emissions from the aircraft engine. The size and duration of the ice supersaturated region, the
140 availability of water vapor for ice crystal growth, and consequently, the sedimentation of these ice
141 crystals within the contrail are also essential considerations (Bock and Burkhardt, 2016). Crucially,
142 the radiative forcing (RF) and the ensuing climate impacts are contingent upon a multitude of

143 meteorological parameters. Additionally, factors such as the albedo and the brightness temperature
144 of the atmosphere in the absence of contrails play a significant role, as outlined by Schumann et
145 al. (2012).

146 Upon reaching the ambient temperature through the process of mixing with the surrounding air,
147 contrails undergo changes in size depending on the ambient humidity. When the ambient relative
148 humidity remains supersaturated concerning ice (RHice >100%), contrails experience growth in
149 ice water content and can remain detectable for up to 5 hours or even longer, as highlighted in
150 various studies (Gierens and Vázquez-Navarro 2018; Schumann and Heymsfield 2017; Bier et al.
151 2017). This extended persistence contrasts with the mean lifetime of contrails, typically noted to
152 be around 2-3 hours (Schumann et al. 2015; Vázquez-Navarro et al. 2015). Contrails, under such
153 conditions, have the potential to disperse and transform into thin cirrus layers. On the other hand,
154 when the ambient relative humidity is not supersaturated concerning ice, contrail ice particles
155 sublimate and dissipate. The timescale of this sublimation and dissipation process is contingent on
156 the sizes of the contrail ice particles and the ambient air RHice (Schumann 2012).

157 Combinations of satellite information and ground-based lidar measurements, such as in the Atlas
158 et al. (2006) case study, showed a lifetime of more than 2 hours and a mean optical thickness
159 (integrated extinction coefficient over a vertical column of unit cross section) of 0.35. Duda et al.
160 (2004) studied the development of contrail clusters over the Great Lakes and derived optical
161 thickness (optical depth, τ) from 0.1 to 0.6 for contrails that lasted several hours (Kärcher et al.,
162 2009). Graf et al. (2012) studied the cirrus cover cycle and observed timescales between 2.3 to
163 4.1 hours for contrail cirrus and 1.4 to 2.4 hours for linear contrails.

164

Figure 3. Phase diagram with mixing lines for aircraft exhaust Adapted from Gierens et al. (2008).
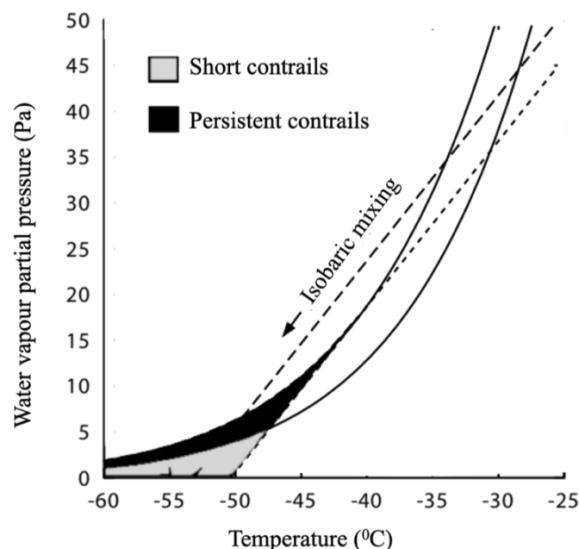
176   There has been ongoing uncertainty regarding whether persistent contrails exclusively form in
177   cloud-free supersaturated areas or if they can also develop within existing cirrus clouds (Burkhardt
178   et al. 2008). Subsequent modeling work (Tesche et al. 2016) suggested that persistent contrails
179   indeed have the potential to form within cirrus clouds. While the formation of contrails is
180   commonly observed in clear skies, they also emerge in conditions where the sky is covered with
181   thin or even subvisible cirrus clouds (Immler et al. 2008).

182   The temperature threshold for contrail formation, known as the SAC threshold, is slightly higher
183   in cirrus clouds compared to clear air (Gierens, 2012). This difference is attributed to the additional
184   humidity introduced by the ice water content (IWC) from cirrus clouds (Verma and Burkhardt
185   2022). In situ measurements have indicated high ice supersaturation both inside and outside cirrus
186   clouds (Comstock et al. 2004). Moreover, observational evidence suggests that contrails embedded
187   within cirrus clouds are not significantly thinner than contrails forming in clear air (Poellot et al.
188   1999).

189   A reliable estimation of the radiative effects stemming from contrail cirrus relies heavily on their
190   optical properties, which are intricately linked to their microphysical properties and age, as well
191   as their geographical distribution. The microphysical characteristics of contrail cirrus at various
192   plume ages, as observed in diverse airborne campaigns, have been systematically compiled and
193   detailed (Schröder et al. 2000; Schumann et al. 2017; Chauvigné et al. 2018). Fresh contrails,
194   typically observed in plumes around 2 minutes old, exhibit distinct features, including an ice
195   crystal number concentration reaching thousands per cubic centimeter and ice crystals measuring
196   up to a few micrometers in diameter. This characterization is consistent with observations (Bräuer
197   et al. 2021a; Petzold et al. 1997). Contrails in their initial 2-5 minutes of existence have been
198   frequently measured (Voigt et al. 2011; Gayet et al. 2012). The distinctive feature of these young
199   contrails lies in their notably high ice crystal number concentration of small ice particles, making
200   them easily discernible from natural cirrus formations. However, contrails often coexist with
201   natural cirrus and may be incorporated into thin or subvisible cirrus (Kübbeler et al. 2011; Gierens
202   2012; Unterstrasser et al. 2017). This coexistence poses a challenge in distinguishing between aged
203   contrails and natural cirrus, complicating efforts to clarify the contribution of contrail cirrus to the
204   radiative balance. Contrail cirrus is characterized by a low ice water content (IWC) ranging from
205   0.1 to about 10 mg m^{-3}, a feature it shares with natural cirrus of in-situ origin, as observed by
206   Schumann et al. (2017). Ice crystals within these clouds have formed and enlarged in an ice-cloud
207   environment (Luebke et al., 2016; Krämer et al. 2020). In contrast to contrail cirrus and in situ-
208   origin cirrus, cirrus clouds initiating from liquid often yield a higher IWC since their ice crystals
209   originally form as liquid drops (Krämer et al., 2016, 2020) in a warmer atmosphere with an ambient
210   temperature exceeding 235 K (-38°C), particles undergo freezing as they are lifted into the cirrus
211   temperature region of the atmosphere.

212   Chauvigné et al. (2018) applied a method based on principal component analysis to differentiate
213   between particles in contrail cirrus at various stages and those observed in natural cirrus during
214   the CONCERT 2008 campaign (Voigt et al., 2010). The success of the campaign stemmed from
215   the fact that contrails sampled during the CONCERT initiative were relatively young and exhibited
216   greater distinctiveness compared to natural cirrus formations. Despite this success, the
217   comprehensive acquisition of all necessary optical and microphysical parameters proved
218   challenging during single aircraft campaigns, limiting the widespread application of this method.
219   The CONCERT dataset is relatively small, encompassing approximately 4.0 hours of sampling
220   time in total (Kübbeler et al. 2011). A commonly held assumption regarding the formation and

evolution conditions of contrail cirrus is that it tends to persist particularly in ice-supersaturated regions (ISSRs) (Kärcher 2018).

The collective presence of commercial, military, and other aircraft contributes to a global increase in cloudiness, primarily facilitated by the formation of persistent contrails when the surrounding atmosphere reaches supersaturation. Contrail cirrus exhibits both cooling and warming effects, with the nighttime impact being predominantly warming. Previous assessments of aviation's influence on climate (IPCC 1999; Lee et al. 2009; Brasseur et al. 2016) were limited by the challenge of accurately quantifying the role of cloudiness arising from aging and spreading contrails (Minnis et al., 2013). The formation of a persistent contrail necessitates ice-supersaturated conditions along the aircraft's flight path. The life cycles of contrail cirrus are contingent upon the temporal and spatial scales of ice-supersaturated regions, which exhibit high variability in the troposphere and tropopause region (e.g., Lamquin et al., 2012; Irvine et al., 2013; Bier et al., 2017). Estimating the impact of contrail cirrus on upper tropospheric cloudiness requires the simulation of complex microphysical processes, contrail spreading, overlap with natural clouds, radiative transfer, and interaction with background cloudiness (Burkhardt et al., 2010).

The ERF of contrail cirrus was estimated for 2011 (relative to an atmosphere without contrails) as 50 mWm^{-2} by Boucher et al. (2013), with uncertainty ranging from 20-150 mWm^{-2}. Lee et al. (2021) presented a new estimate derived from the outcomes of global climate models implementing process-based contrail cirrus parameterizations. Recent analyses by Lee et al. (2021) of the current aviation fleet emissions evaluate the ERF through 2018 as 57 mWm^{-2}, with an uncertainty range of 17-98 mWm^{-2}. Given the constrained number of independent estimates, it becomes necessary to gauge uncertainty by relying on the sensitivities of pertinent processes and considering uncertainties associated with the underlying parameters and fields. Due to the small number of independent estimates, the uncertainty must be estimated from the sensitivities of the respective processes and the uncertainty in the underlying parameters and fields. Kärcher et al. (2015) observed that contrails are created in the early exhaust plumes of airplanes during cruising. This occurs when a large number of supercooled water droplets are activated and freeze into ice particles. At cruising altitudes, the atmospheric relative humidity (RH) typically falls too low to support the presence of liquid water droplets. However, it is conducive to the existence of ice-phase particles (Gettelman et al., 2006; Lamquin et al., 2012). Therefore, freezing must occur shortly after droplet formation within the moist exhaust plume to produce persistent contrails. Appleman (1953) proposed a critical requirement for contrail formation, suggesting that a significant amount of aerosol particles in the plume act as centers for water condensation (referred to as the "water-saturation constraint"). The formation of contrails also has a visibility constraint, which estimates a minimum number of nucleated ice particles in the contrails at around 10^4 cm^{-3} within a plume age of 0.3s for a small-scale research aircraft (Kärcher et al., 1996). These are the crucial constraints for contrail formation.

2.2 Transition of contrails into contrail cirrus and contrail-cirrus-soot interaction

Contrail cirrus consists of elongated contrails trailing high-altitude aircraft and thin cirrus patches formed by the dispersion of persistent contrails. The morphology of contrails evolves based on factors such as humidity, shear, stratification, waves, turbulence, and radiative heating. Contrails, individually and collectively, interact with other cirrus formations, giving rise to what is termed "contrail cirrus" (Schumann and Wendling, 1990). The total extinction is less pronounced when contrails overlap due to humidity competition. Consequently, the climate impact does not always

266 exhibit a linear correlation with air traffic density (Unterstrasser and Sölch, 2012; Bickel et al.,
267 2020). The transformation of a single contrail into a contrail cirrus is observable during aircraft
268 spiral flights, as depicted in Figure 4 (Haywood et al., 2009). "Contrail outbreaks" describe
269 scenarios where numerous aged and young contrails coexist, often spanning expansive areas within
270 the same airspace (Duda et al., 2001).

271 Soot emissions, composed of black carbon particles from aviation, have the potential to alter cirrus
272 properties independently of contrail processing, leading to the formation of "soot cirrus" (Lee et
273 al., 2010). Climate impact assessments of aviation-induced soot cirrus remain inconclusive due to
274 uncertainties in soot abundance and their ice-nucleating properties (Gettelman and Chen, 2013;
275 Zhou and Penner, 2014; Righi et al., 2021). Increased concentrations of small-sized cirrus particles
276 resembling aviation soot emissions have been detected in cirrus regions with dense air traffic
277 (Kristensson et al., 2000). It remains uncertain whether the soot enters the ice during the initial
278 nucleation process or at a later stage through scavenging.

279 The sublimation of cirrus particles containing soot and sulfate may lead to the formation of soot
280 aggregates that can potentially act as efficient ice nuclei. A cirrus pattern observed near Munich,
281 Germany, on November 3, 2012, displayed characteristics suggesting an association with aged
282 soot plumes. The cirrus observed between 9.1 and 9.5 km in height, 8-10 km wide, and 35-50 km
283 long, exhibited a distinctive pattern resembling parallel line clouds. Back trajectories indicated that
284 soot was emitted upstream approximately 12 hours before the event by aircraft. The air ascended,
285 forming a cirrus about 4 hours before the event, lasting for about 1-2 hours before subsiding or
286 sublimating. Analyses propose that this could be cirrus formed on preactivated aircraft soot, but
287 certainty is limited, and it cannot be ruled out that the same pattern might have formed without air
288 traffic.
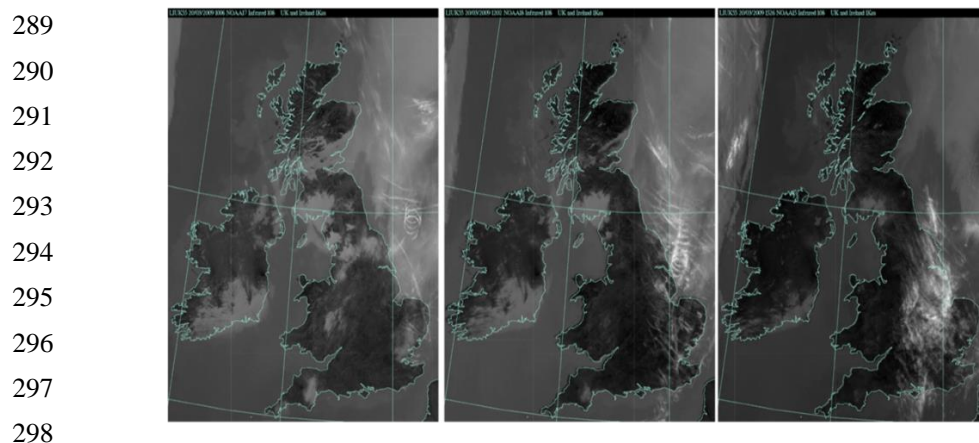
Figure 4. Evolution of contrail cirrus over 1, 3, and 6.5 hours. Contrail cirrus is identified by bright
white areas with low infrared (10.8 mm) brightness temperature. The satellite scenes are from
NOAA AVHRR for 3 UTC times: (left) 1006 (age after emission = 1 hour), (middle) at 1202
(elapsed time: 3 hours), and (on the right) 1526 (elapsed time: 6.5 hours). Figure adapted with
permission from Haywood et al. (2009). The license is provided by John Wiley and Sons and the
Copyright Clearance Center (License Number 5603970305771)

305   Urbanek et al. (2018) conducted measurements of ice clouds over Europe using an airborne remote
306   sensing instrument. They observed a particular group of clouds characterized by elevated
307   depolarization ratios, suggesting altered crystal habits, and lower ice supersaturation, indicating
308   modified ice formation. The researchers demonstrated that these changes were not caused by
309   condensation trails within the clouds, temperature variations, or atmospheric dynamics.
310   Interestingly, these clouds were found to have formed in the air originating from heavily trafficked
311   aviation routes. As a result, their findings could potentially represent the initial evidence of this
312   indirect process.

313   Kärcher et al. (2021) applied an advanced cirrus column model to investigate the impact of aircraft-
314   emitted soot particles on the formation of cirrus clouds. These particles are released when ice
315   crystals sublimate at the end of the lifespan of contrails and contrail cirrus. By incorporating cloud
316   simulations with a measurement-based representation of soot-induced ice formation, the
317   researchers noticed that only a small fraction (less than 1%) of the soot particles were able to
318   contribute to the formation of cloud ice through homogeneous freezing of liquid aerosol droplets.
319   Subsequently, cirrus clouds impacted by soot and those formed homogeneously presented no
320   significant differences in terms of their optical depth. These outcomes suggest that climate models
321   may have overestimated the global radiative forcing resulting from interactions between aircraft
322   soot and large-scale cirrus clouds. The insights gained from Kärcher et al.'s research provide a
323   more comprehensive understanding of the underlying processes, offering a valuable basis for
324   improving climate model parameterizations and guiding specific field observations to enhance
325   accuracy in climate modeling.

326   Natural cirrus clouds and contrails collectively cover around 30% of the Earth's mid-latitudes and
327   up to 70% of the tropics (Wolf et al., 2023). Given their widespread presence, cirrus clouds
328   significantly impact the Earth's energy budget, resulting in a warming net radiative effect,
329   encompassing both solar and thermal infrared radiation. However, whether the instantaneous
330   radiative effect (RE), at times equivalent to radiative forcing, is positive or negative depends on
331   several factors, including microphysical, macrophysical, and optical properties, as well as the
332   radiative characteristics of the surrounding environment. The complexity is further heightened by
333   the often-unknown shape of actual ice crystals, rendering ice clouds one of the least understood
334   components in the Earth's radiative budget. Wolf et al. (2023) explored the dependency of cirrus
335   RE on eight parameters: solar zenith angle, ice water content, ice crystal effective radius, cirrus
336   temperature, surface albedo, surface temperature, cloud optical thickness of an underlying liquid
337   water cloud, and three different ice crystal shapes.

2.3 Evolution of contrails and stages of aviation-induced cloud evolution

339   The review by Paoli and Shariff (2016) examined the primary physical processes and simulation
340   efforts involved in four distinct phases of contrail evolution. These phases are commonly
341   categorized as the jet, vortex, vortex dissipation, and diffusion phases. Contrail evolution is
342   conveniently divided into these four regimes for clarity (Gerz et al., 1998) (see Fig.5).

343   In the initial seconds after emission (the jet regime), the vortex sheet shed by the wings rolls up
344   into a pair of counter-rotating vortices known as the primary wake. Simultaneously, newly formed
345   ice crystals in the engine exhaust become entrapped around the cores of these vortices. Following
346   this, in the minutes that follow (the vortex regime), the vortices descend into the atmosphere due
347   to their mutually induced downward velocity. The descent of vortices effects in a contrast in
348   density between the air contained within the vortices (within an oval-shaped region) and the

349 ambient air. This process leads to the generation of vortices with opposite signs (in a stable
350 stratified atmosphere) along the oval boundary. The vorticity shed in the upward direction gives
351 birth to a "secondary wake." Within this secondary wake, a portion of the exhaust gases and ice
352 particles becomes incorporated.

353

354
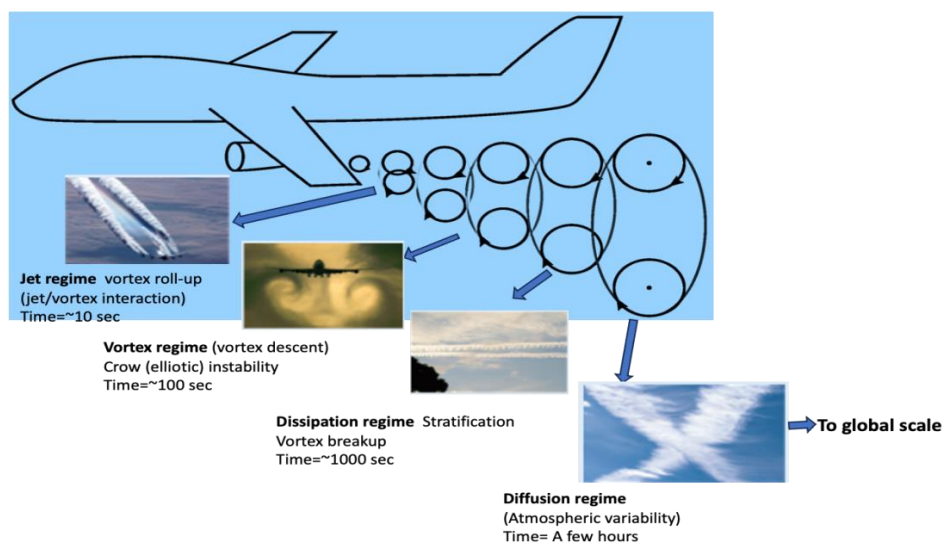
Figure 5. Classification of aircraft wakes evolution into four regimes. Adapted from Paoli and
Shariff (2016).

357 Within the regime of vortex dissipation, the primary vortex pair and secondary vorticity
358 disintegrate and disperse, releasing both exhaust and ice crystals that eventually endure
359 sublimation. Ice crystals released in the secondary wake can endure for a longer duration due to
360 the lower temperature. In the fourth regime, known as the diffusion regime, the horizontal and
361 vertical spreading of the contrail is influenced by atmospheric turbulence, particle sedimentation,
362 radiative processes, and wind shear until complete mixing takes place, typically within a few hours.
363 Figure 6 illustrates the processes that influence the various stages of contrail formation. Exhaust
364 plumes, generated by burning fuel-air mixtures at high temperatures and pressure within turbofan
365 jet engines, contain both gaseous and particulate matter. In the freely expanding and cooling
366 plumes (jet regime), particle types include emitted soot particles and aqueous aerosol particles
367 formed within the exhaust, along with entrained ambient aerosol particles. In scenarios where
368 turbulent mixing occurs, leading to cooling and generating plume supersaturation over liquid
369 water, a significant number of plume particles undergo transformation into water droplets
370 (depicted as gray circles in Fig. 6).

371 Water droplets rapidly freeze and increase in size by absorbing water vapor from their
372 surroundings, eventually leading to the formation of a visible contrail. This occurs when the
373 ambient temperature drops below the formation threshold. In exhaust rich in soot, most droplets
374 contain soot inclusions. While droxtals, frozen water droplets with faceted surfaces, and hexagonal
375 prisms and columns likely emerging from them may offer a realistic depiction of small ice crystals
376 in fresh contrails, there is currently no direct observational evidence for their specific shapes.

377   Plumes from multiple aircraft engines combine with the two wingtip vortices, creating an
378   inhomogeneous wake. The subsequent evolution of ice crystals is contingent upon fluid-dynamical
379   processes, particularly in the vortex regime. The downward movement of the vortex pair warms
380   the surrounding air, resulting in the sublimation of ice crystals in the lower portion of the wake. A
381   small fraction of contrail is amplified by the detrainment of air from the lower wake. Ice crystals
382   present in the upper wake continue to grow by the uptake of entrained ice-supersaturated ambient
383   water vapor. A few minutes past emission, the organized flow pattern collapses and mixes with
384   ambient air (dissipation regime).

385

386

387
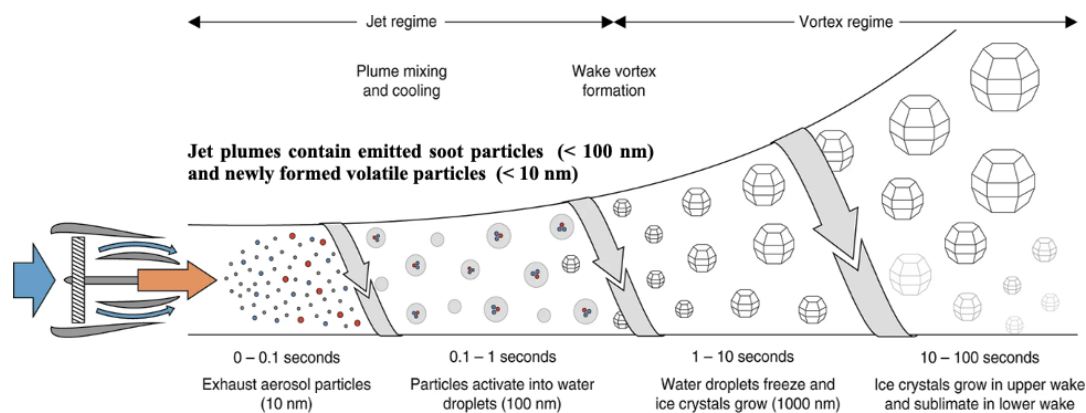
388

389

390   **Figure 6.** Processes influencing the contrail formation stage. Figure adopted with permission from
391   Kärcher (2018). (Licensed under CC BY 4.0)

392

393   **2.4 Contrail coverage**

394   The radiative forcing (RF) for contrails, as determined by Lee et al. (2010), is defined by the
395   product of contrail coverage and optical depth. For a single contrail segment, this product equates
396   to total extinction. However, defining contrail coverage presents challenges for several reasons.
397   Assessing contrail coverage separately from optical depth introduces difficulties. The
398   identification of young contrails versus other cirrus clouds often relies on their distinctive line
399   shape. Yet, using geometric characteristics for contrail coverage classification introduces
400   uncertainty, particularly when contrails undergo deformation or shape changes (Mannstein et al.,
401   1999). Only a small fraction of all linear contrails is detectable from satellites (Kärcher et al., 2009;
402   Mannstein et al., 2010; Minnis et al., 2013).

403   Earlier studies examined global contrail coverage using regional satellite observations, estimating
404   potential contrail coverage based on specific temperature and humidity data and traffic density
405   (Sausen et al., 1998). The integration of observations to achieve hemispheric coverage has only
406   recently become available (Duda et al., 2013). The coverage by contrail cirrus may be significantly
407   higher than determined by line-shaped contrails, and uncertainty factors around an order of 10

408 have been reported (Burkhardt and Kärcher, 2011). However, this ratio is highly uncertain due to
409 detection issues. Burkhardt and Kärcher (2011) conducted a quantification of contrail cirrus using
410 the ECHAM contrail cirrus global climate model (CCmod), which incorporates a subgrid-scale
411 cloud class representing young contrails. This model captures the life cycle of artificial clouds and
412 simulates their global coverage, along with the changes in natural cloudiness they induce. Their
413 calculations revealed contrail cirrus coverage to be approximately 0.23%. Similar results were
414 obtained from recent attempts to quantify contrail cirrus using MODIS data, accounting for more
415 diffuse contrail contributions (Minnis et al., 2013).

416 Schumann (2012) developed the Contrail Cirrus Prediction (CoCiP) tool based on a Lagrangian
417 approach. In this model, global contrail coverage is computed by combining the optical depth (τ)
418 contributions from individual contrails and ambient cirrus, counting fractions of areas where
419 contrails cause the optical depth of the total cirrus to surpass a specific threshold (Schumann 2012).

420 Contrails not only augment cloud coverage but also thicken existing cirrus, consequently
421 influencing coverage (Minnis et al., 2013; Schumann and Graf, 2013). This thickening occurs by
422 generating more ice particles with smaller effective radii at constant ice water content (Kristensson
423 et al., 2000). While it is acknowledged that contrails consume humidity and may reduce natural
424 cirrus (Burkhardt and Kärcher 2011; Unterstrasser and Görsch 2014; Schumann et al., 2015; Bickel
425 et al., 2020), the prevailing evidence suggests that the thickening effect caused by numerous
426 additional small ice crystals tends to dominate.

427
2.5 Contrail ice crystal nucleation

429 Kärcher and Yu (2009) systematically investigated the relationship between nucleated contrail ice
430 crystal numbers and soot particle emissions. In exhaust rich in soot, there is a nearly proportional
431 increase in both ice crystal and soot particle numbers. Close to the contrail threshold, the formation
432 of ice crystals is limited as the low plume supersaturation hinders the activation of water on soot
433 particles, resulting in only a few ice crystals forming. Under conditions rich in soot, the quantity
434 of ice crystals reduces by about one hundred times compared to soot-poor conditions, reaching
435 constant low levels regulated by the number of particles present in the contrail environment. In
436 soot-poor exhaust at low ambient temperatures, there is an increase in ice crystal numbers due to
437 the activation of water and subsequent freezing of abundant aqueous plume particles. Figure 7
438 illustrates the ice crystal number emission index (per kilogram of fuel burnt) in the jet regime,
439 correlating with the number emission index of emitted soot particles as simulated by a parcel model
440 (Kärcher and Yu, 2009). Two sets of results are presented, one for an ambient temperature (T)
441 close to a contrail formation threshold temperature, $\Theta \approx 225$ K (-48°C), commonly encountered in
442 extratropical cruise conditions, and another for a lower temperature of Θ -12 K ≈ 213 K (-60°C).
443 At intermediate ambient temperatures, nucleated ice crystal numbers increase due to enhanced
444 water activation of either soot or ultrafine aqueous plume particles.

445 The hatched area in Figure 7 represents the approximate range of current in-flight soot emission
446 indices. In exhaust rich in soot, the number of soot particles capable of water activation and
447 freezing increases with decreasing ambient temperature. This, in turn, raises plume cooling rates
448 and levels of plume supersaturation over liquid water. As the ambient temperature (T) approaches
449 the contrail formation threshold (Θ) in soot-poor exhaust, ambient aerosol particles mixed into
450 exhaust plumes become the sole source of contrail ice crystals. This is because fewer plume

451   particles can be activated due to declining plume supersaturation. The number concentrations of
452   ambient particles in contrails are significantly lower than current levels of soot emissions.

453   The plume cooling rate plays a crucial role in determining the timing of water activation of
454   entrained ambient particles and, consequently, the number of ice crystals derived from them
455   (Kärcher 2015). In soot-poor exhaust, a substantial number of ultrafine aqueous plume particles
456   are formed in the fresh exhaust, especially if the fuel contains condensable vapors besides water
457   vapor. These small particles are anticipated to contribute significantly to ice crystal formation at
458   low ambient temperatures well below average values at cruise levels (T ≈ 218 K in the extratropic
459   and T ≈ 228 K in the tropics). If the formation of ultrafine particles cannot be mitigated, ice crystal
460   numbers are expected to be lowest in an intermediate range of soot emissions, specifically between
461   10^{13} and 10^{14} (kg-fuel)$^{-1}$.

462   The ice crystal number (Ni) holds significant importance in the context of contrails formation. Ni
463   quantifies the concentration of ice crystal particles present in the surrounding atmosphere. The
464   significance of Ni in contrail formation lies in its direct influence on various contrail properties.
465   Key aspects such as contrail persistence, the extent of spreading, and the optical characteristics of
466   contrails are closely tied to the ice crystal number (Ni). In essence, Ni serves as a fundamental
467   factor in understanding and characterizing contrail behavior and its impact on the atmosphere. A
468   higher Ni value implies a higher concentration of ice particles in the contrail, which can have
469   several implications, for instance, contrails with a higher Ni tend to persist for longer periods of
470   time. This means they remain visible in the sky for extended durations before dissipating or
471   spreading. Higher Ni values are associated with greater contrail spreading. As the ice particles in
472   the contrail interact with the surrounding atmospheric conditions, they can spread out and cover a
473   larger area, which may lead to contrail cirrus. The optical properties of contrails, for instance, their
474   brightness and ability to scatter sunlight, are affected by the ice crystal number. Higher Ni values
475   can result in brighter and more reflective contrails, which can contribute to increased cloudiness
476   and affect the Earth's energy balance.

477   The signs of variation in the number of ice crystals refers to the alteration in the ice particle
478   concentration within a contrail, such as increased ice particle concentration in the contrail, greater
479   persistence, and spreading of the contrail. Increased optical effects, such as increased brightness
480   and reflectivity. The decreased ice crystal particle concentration in the contrail leads to reduced
481   persistence and spreading of the contrail, and weaker optical effects. These variations in Ni may
482   occur due to several factors, comprising changes in atmospheric conditions, aircraft engine
483   emissions, and the presence of ice nuclei or other particles that impact ice particle formation.

2.6 Stages of aviation-induced cloud evolution and spreading stage

485   The microphysical and optical characteristics of ice crystals within contrails undergo alterations
486   as they disperse or transform into contrail cirrus, contingent upon the prevailing meteorological
487   conditions and microphysical processes (Fig. 8). Over time, persistent contrails undertake a
488   transformation from their initial linear form to become contrail cirrus. In regions of heavy air
489   traffic, these contrail cirrus formations overlap and merge, giving rise to extended layers of ice
490   clouds characterized by alterations in shape, depth, and longevity. These patterns differ from
491   natural cirrus clouds in terms of microphysical, optical, Additionally, geometric properties also
492   play a role. The ice supersaturated layers that sustain these properties exhibit variations in both
493   vertical structure and horizontal extent, impacting the exchange of water molecules between vapor
494   and ice phases within them. Collectively, these factors contribute to the radiative forcing (RF)

495 potential of aviation-induced cirrus (AIC). Figure 8 illustrates the augmentation in cloud coverage
496 area attributed to the vertical shear of horizontal wind components.

497 The turbulent mixing or entrainment processes result in a gradual reduction (dilution) of ice crystal
498 concentrations over time. The sizes of ice crystals grow through the absorption (deposition) of
499 water vapor from layers that are supersaturated with ice. Continuous deposition growth causes
500 deviations in the shapes (habits) of ice crystals from their initial isometric forms.
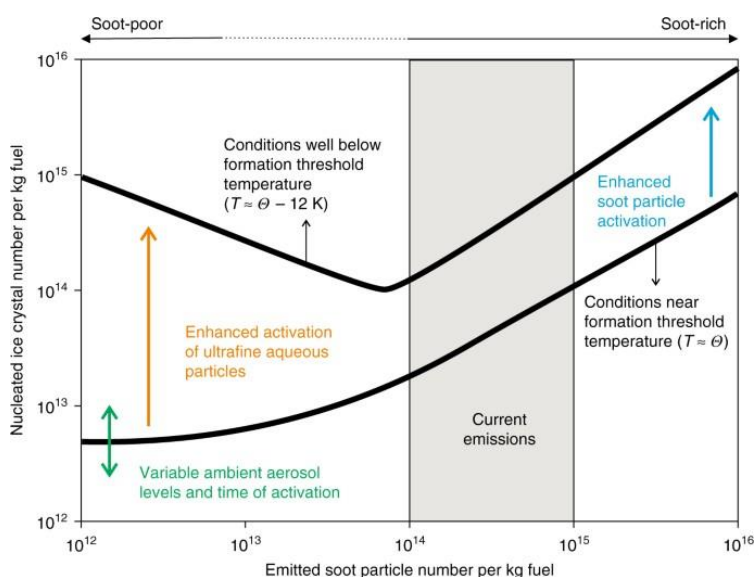
514 **Figure 7.** Nucleation of ice crystals in jet aircraft exhaust plumes. Figure adapted with permission
515 from Kärcher (2018). (Licensed under CC BY 4.0)

516 The shapes and sizes of ice crystals in cirrus clouds significantly impact their growth rates, fall
517 speeds, and optical properties. Larger ice crystals (>30 micrometers) tend to settle due to gravity
518 with fall speeds exceeding 100 meters per hour and are more likely to sublimate in warmer or drier
519 environments. Smaller ice crystals remain suspended around the flight levels due to their negligible
520 fall speeds, provided that some degree of supersaturation can be maintained, which depends on the
521 prevailing meteorological conditions.

522 The efficiency of sedimentation, the process by which ice crystals fall from clouds, is influenced
523 by the depositional growth rate, which in turn is affected by ice supersaturation, the rate of air
524 cooling, and the characteristics of the ice crystals themselves, including their size, shape, and
525 number concentration. Sedimentation increases the vertical extent of cirrus clouds, enhancing their
526 spreading rate and coverage under sheared flow conditions.

527 **2.7 Lessons learned from observations of contrails and their properties**

528 Contrails, as well as cirrus clouds, are frequently observed in air that lacks saturation (Kübbeler et
529 al., 2011; Krämer et al., 2009). The prevailing explanation suggests that these clouds consist of
530 large ice particles formed under supersaturated conditions, which then descend to lower and drier

531 levels, undergoing slow sublimation. Notably, instances of contrails and contrail cirrus have been
532 documented in ice-sub-saturated air across various scenarios, extending beyond dedicated contrail
533 research flights (Schumann et al., 2017; Voigt et al., 2011; Kübbeler et al., 2011; Gayet et al.,
534 2012; Chauvigné et al., 2018). Such observations have been derived not only from contrail-specific
535 research endeavors but also from In-service Aircraft for a Global Observing System (IAGOS)
536 commercial aircraft data collected in the North Atlantic region (Petzold et al., 2017).

537 Apart from a high number of small contrail ice particles, large particles (ice particle diameter
538 greater than 100 µm) were also detected but at relatively low concentrations (Voigt et al., 2010).
539 Such large ice crystals were also observed in contrail cirrus during the ML-CIRRUS (Midlatitude
540 Cirrus experiment) campaign (Voigt et al., 2017). However, attention to contrail cirrus in ice-sub-
541 saturated environments and the role that large ice particles play in contrail cirrus was raised by
542 Kübbeler et al. (2011) and Schumann (2012).
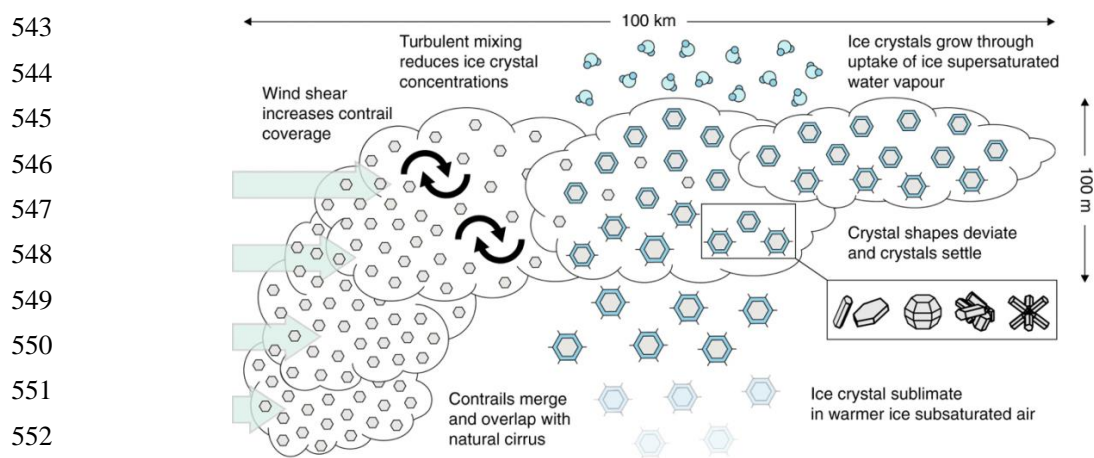
Figure 8. Influential factors in aircraft-induced cloud formation. Figure adopted with permission
from Kärcher (2018). (Licensed under CC BY 4.0)

557 Kübbeler et al. (2011) suggested that the subsaturation observed in contrail cirrus during the
558 CONCERT campaign is caused by the sublimation of large ice particles that may have fallen from
559 higher altitudes after forming under ice supersaturated regions (ISSRs). However, due to the
560 limited contrail cirrus data available, it is difficult to confirm whether contrail cirrus commonly
561 occurs in ice-subsaturated environments.

562 Li et al. (2023) explored an extended dataset derived from 14.7 hours of cirrus cloud sampling
563 conducted at a frequency of 1 Hz, with a maximum speed of approximately 290 m s^{-1}, obtained
564 during the ML-CIRRUS 2014 campaign. Utilizing readily available parameters that characterize
565 cirrus microphysical properties-including ice number concentration, ice crystal sizes, and ice water
566 content (IWC)-they employed a more straightforward statistical method to distinguish aviation-
567 induced cirrus from natural cirrus, in contrast to the approach adopted by Chauvigné et al. (2018).
568 It consists of the SAC, covering the most common aircraft cruising altitude range, and a recently
569 developed algorithm for detecting aircraft exhaust plumes (Mahnke et al., 2022) to identify
570 matured contrail cirrus (>0:5 h lifetime; Voigt et al., 2017; Schumann et al., 2017) and natural

571 cirrus. Contrail cirrus showed sharp differences from natural cirrus during the stages of formation
572 and in the corresponding microphysical properties and occurrence conditions.

573 **3 Modeling of Contrails and their Impacts**

574 Local-scale process and fluid-dynamic models systematically explore how plume turbulence and
575 wake dynamics affect nucleation and properties of contrail ice crystals and how predictions of
576 nucleated ice numbers and sublimation losses relate to aircraft measurements. Cloud-resolving and
577 regional models driven with meteorological boundary conditions and combined with optical
578 parameterizations capturing the short-wave response of µm-sized ice crystals analyze large
579 atmospheric regions based on collocated aircraft and satellite measurements to better judge AIC
580 RF and the radiative significance of natural cirrus perturbed by contrails (Kärcher 2018). For ice
581 cloud parameterizations, instrumental challenges pose significant limitations in the measurements
582 of the microphysical and optical properties of contrail cirrus. This heightens the role of models
583 (Table 1) in providing RF estimates. For simulating ice nucleation and sublimation robust
584 predictions of climate changes that result from aircraft-induced clouds rely significantly on the
585 ability to transfer the understanding of the formation and evolution process of AIC outlined above
586 into models that are not capable of treating the formation stage explicitly due to a lack of spatial
587 or temporal resolution. This goal can be reached by allying findings from observations with local-
588 scale, process-oriented models.

589

590 **Table 1.** Modeling the complexities of aircraft-induced cloud radiative effects (Adapted from
591 Kärcher 2018).

Model scale	Spatial resolution		Contrail stages	Major challenges	Approach/solution
	Horizontal	**Vertical**			
Local	<10 m	<10 m	Formation stage	Ice crystal number and size distribution	Turbulence microphysics coupling
Regional	<1000 m	<100 m	Spreading stage	Radiative flux changes and interaction with natural clouds	Contrail to contrail cirrus transition
Global	<1000km	<1km	Full life cycle	Ice crystal formation and ice supersaturation	Parameterization and high resolution

Improvements in a hierarchy of local- to global-scale models to be realized in conjunction with observations providing data for cloud and radiation parameterization development and overall model validation.

592
593

594 **3.1 Modeling of individual contrails**

595 Individual contrails have been studied by various authors through approaches ranging from
596 simplified parameterizations to more complex numerical models. Parameterization approaches
597 normally depend on simplified assumptions to estimate contrail properties based on simplified
598 atmospheric and emission conditions. On the contrary, more sophisticated numerical models, such
599 as the Contrail Cirrus Prediction model (CoCiP), utilize detailed representations of atmospheric
600 processes, ice particle growth, and radiative transfer to simulate the formation and evolution of
601 contrails.

602 **3.1.1 Contrail Cirrus Prediction Tool (CoCiP) for individual contrails**

603 Schumann et al. (2017) compiled a dataset of contrail properties from various sources, including
604 previous publications, additional information gathered from experimenters, reanalysis of existing
605 data, and comparisons with the CoCiP database. The dataset expands upon the work of Schumann
606 and Heymsfield (2016) by incorporating data from the ML-CIRRUS campaign (Voigt et al., 2016).
607 The data includes both in-situ measurements of contrails, such as ice particle size spectra obtained
608 using optical particle spectrometers (Baumgardner et al., 2011; Wendisch and Brenguier, 2013),
609 and remote sensing data from ground-based and airborne lidar, spectroradiometers, satellites,
610 cameras, and visual observations. Remote sensing data provides information on contrail properties
611 such as width and optical depth (Spinhirne et al., 1998; Duda et al., 2004).

612 **3.1.2 MIT Aircraft Plume Chemistry, Emissions, and Microphysics Model (APCEMM)**

613 APCEMM is applied to assess the impact of non-linear plume chemistry and to deliver an initial
614 estimate of the effects of contrails on atmospheric chemistry. Accurately determining the intricate
615 relationship between contrail microphysics and chemistry often necessitates the use of costly large
616 eddy simulations (LESs). APCEMM, through simplified assumptions about plume dynamics,
617 strives to close the disparity between Gaussian plume models and LESs, as outlined by Fritz et al.
618 (2020). APCEMM simulates the growth and chemical progression of an individual aircraft plume.
619 It computes chemical concentrations and aerosol characteristics for a two-dimensional cross-
620 section of the plume, angled perpendicular to the flight path. Dynamics, chemistry, and
621 microphysics are explicitly modeled within the plume, using two different approaches depending
622 on the age of the plume.
623
624 **3.1.3 NASA's global model for evaluation of individual linear contrails**

625 The NASA Ames Research Center developed a computationally efficient aircraft contrail model
626 designed to simulate aircraft-induced contrail formation. This model relies on the Appleman
627 criterion and operates under static atmospheric conditions (Sridhar et al., 2010; Neil et al., 2010).
628 Subsequently, researchers from NASA Ames extended this model to simulate the dynamic
629 transport of contrails by incorporating a Lagrangian dispersion model and a cloud microphysics
630 model (Li et al., 2013). The computational methods employed are grounded in well-established
631 approaches utilized in other aircraft contrail models (Pruppacher and Klett, 2000; Schumann et al.,
632 1995). In comparison with models from Stanford (Naiman et al., 2009; Naiman et al., 2011;
633 Jacobsen et al., 2011) and DLR (Burkhardt and Kärcher, 2009; Burkhardt and Kärcher, 2011; Bier
634 and Burkhardt, 2022), this dynamic contrail model diverges primarily in two aspects: (1) It
635 excludes the initial contrail ice particles down-wash process caused by airplane wake vortex
636 turbulence. This process, typically lasting less than a minute, is crucial in determining contrail ice
637 nucleation, initial contrail ice particle sizes, and displacements through a complex fluid dynamic
638 process dependent on atmospheric, aircraft, and fuel parameters. In this study, the average initial
639 ice particle size is predefined, and the initial contrail location is set based on the cell where contrail
640 formation conditions are met. (2) The results from this model do not yet include additional
641 radiative forcing caused by aircraft contrails. The researchers are in the process of adding a contrail
642 radiative forcing module capable of computing the total aircraft contrail radiative forcing using
643 inputs from the model, such as ice particle size and linear contrail cloud cover area.

644 **3.1.4 DLR's ICON-LEM regional model**

645 Verma and Burkhardt (2022) developed and implemented a model for contrail formation into the
646 ICON-LEM (ICOsahedral Non-hydrostatic Large-Eddy Model; Zängl et al., 2014; Dipankar et al.,

647 2015). This model includes parameterizations for ice nucleation in the jet phase and ice crystal
648 loss during the contrail's vortex phase. It facilitates the investigation of modifications to cirrus
649 clouds resulting from contrail formation. ICON is the new German Numerical Weather
650 Prediction/Climate Model co-developed by DWD and MPI. It solves a set of equations on an
651 unstructured triangular grid based on successive refinement of a spherical icosahedron (Zängl et
652 al., 2014). The model asserts high horizontal resolution coupled with a vertical resolution of
653 approximately 150 m in the upper troposphere, enabling the resolution of pertinent cloud
654 processes. Within ICON-LEM, a contrail scheme has been developed and implemented,
655 incorporating the parameterization of contrail ice nucleation as proposed by Kärcher et al. (2015)
656 and accounting for the survival of ice crystals within the vortex phase. (Unterstrasser, 2016), to
657 study changes in cloud variables due to contrail formation within cirrus. Contrail formation,
658 dependent on atmospheric as well as aircraft and fuel parameters, is calculated, and contrail ice
659 nucleation and ice crystal loss in the contrail's vortex phase are estimated.

3.1.5 Large-eddy simulations covering the entire life cycle, from initiation to termination

661 Lewellen et al. (2014) outlined the utilization of large-eddy simulations with size-resolved
662 microphysics to model persistent aircraft contrails and the resulting contrail-induced cirrus clouds.
663 These simulations aim to depict the dynamic evolution of contrails, spanning from a few wing
664 spans behind the aircraft to their dissipation over an extended period. The emphasis of the study
665 lies in the modeling approach, discussing the development of schemes for efficient numerical
666 computation. The authors introduced dynamic local ice binning and updating, along with coupled
667 radiation, to accurately capture microphysical processes and radiative properties within individual
668 columns. The paper also addresses the challenge of maintaining realistic ambient turbulence over
669 extended simulation times, proposing a "quasi 3D" approach as a computationally feasible
670 approximation of the full dynamics, allowing for exploration across a broader parameter space.

671 Key insights from the simulations highlight the notable impact of ice crystal number loss resulting
672 from competition among different crystal sizes, influencing both young contrails and aging contrail
673 cirrus. The sensitivity of contrail properties to the initial number of ice crystals decreases over
674 time, highlighting the importance of uncertainties in ice crystal deposition coefficients and the
675 Kelvin effect. The influence of atmospheric turbulence on contrail properties and lifetime is also
676 emphasized. Additionally, the paper discusses the effects of ice crystal shape, coupled radiation,
677 precipitation dynamics, and the role of water from fuel consumption in reducing ice crystal loss in
678 colder contrails.

679 Lewellen (2014) provides an extensive analysis encompassing over 200 instances of long-lived
680 contrails, spanning from their formation at several seconds old to their termination. The study
681 investigated the complete lifespan of long-lived contrails originating from a single aircraft. Various
682 factors were explored, including the effective ice crystal number emission index, temperature,
683 relative humidity concerning ice, stratification, shear, supersaturated-layer depth,
684 uplift/subsidence, and coupled radiation. The analysis delved into the scaling behaviors of contrail
685 lifetime, width, ice mass, and surface area. The simulations unveiled contrail lifetimes exceeding
686 40 hours, widths surpassing 100 kilometers, and ice masses exceeding 50 kg per meter of the flight
687 path. The paper identified distinct behavioral regimes influenced by radiative forcing and proposed
688 a simplified model to predict these regimes.

689   Lewellen's simulations provide valuable insights into contrail behavior, shedding light on the
690   significance of crystal number loss mechanisms, the interaction between shear and ice
691   sedimentation, the depth of the supersaturated layer, and the potential impact of "cold" subvisible
692   contrails. The findings from these simulations contribute to estimating the effects of intricate
693   contrail scenarios, formulating mitigation strategies, and enhancing our comprehension of the
694   dynamics of natural cirrus clouds.

695   **3.2 Treatment of contrails in global models**

696   The consideration of contrail cirrus in global climate models has greatly improved in recent years.
697   Despite these advancements, notable uncertainties persist, particularly in the depiction of contrail
698   microphysics and the interaction between contrail-cirrus and cirrus-radiation. As mentioned
699   earlier, the characteristics of young contrail cirrus diverge from those of natural cirrus primarily
700   due to the elevated ice crystal number concentration typical in contrails. Consequently,
701   microphysical process rates in contrail cirrus, influencing its lifespan, can exhibit significant
702   deviations from those observed in natural cirrus. In this section, we examine the treatments of
703   contrail and contrail cirrus in global models. Very few models account for contrails, so our focus
704   is on those models that have been published extensively on contrail impacts, including modeling
705   studies done by the Institute for Atmospheric Physics (DLR), the National Center for Atmospheric
706   Research (NCAR), and Stanford University. The focus is on their modeling approaches and
707   findings. We start with a description of the approach used to treat contrails in these models.

708   **3.2.1 DLR Contrail Cirrus Prediction Model (CoCiP)**

709   CoCiP can be implemented within a GCM and used to study the global distributions of contrails
710   and contrail cirrus (Schumann et al., 2015). The model is specifically crafted for the estimation of
711   contrail cirrus coverage and the analysis of contrail climate impact, particularly in the context of
712   aviation system optimization processes. It is engineered to simulate the entire life cycle of
713   contrails. Contrail segments arise between waypoints along individual aircraft tracks in air masses
714   that are cold and humid enough. The initial characteristics of contrails are contingent upon the
715   specific aircraft involved. The advection and progression of contrails adhere to a Lagrangian
716   Gaussian plume model. This model treats the contrail life cycle using bulk contrail ice physics,
717   incorporating several simplifying assumptions. Notably, the model demonstrates efficiency in
718   handling mixing and cloud processes in a quasi-analytical manner (Schumann, 2012). Mixing and
719   bulk cloud processes are handled by using a quasi-analytical approach or an effective numerical
720   scheme. Contrails become extinct when the bulk ice content endures sublimation or precipitation.

721   The model takes into consideration the impact of both aircraft properties and ambient
722   meteorological conditions. This encompasses established contrail formation thresholds, the effects
723   of advection, turbulent mixing, and the formation of ice mass from both emitted and ambient
724   humidity. The number of ice crystals is contingent upon the quantity of soot particles emitted. The
725   model incorporates simplified approximations for the survival of ice particles in adiabatically
726   sinking wake vortices and the loss of particles in aged contrails (Schumann, 2012).

727   CoCiP (Contrail Cirrus Prediction) depicted in Figure 9 simulates the formation of contrails under
728   specific meteorological conditions, either regionally or globally. Numerical weather prediction
729   data are utilized to determine ambient meteorological conditions through linear interpolation at
730   given positions and times. The model has been effectively employed to simulate contrails in both
731   global and specific cases, and its results have been compared with outcomes from other models
732   and in-situ measurements (Schumann, 2012).

3.2.2 DLR version of the ECHAM5-HAM model

733

734 The global climate model ECHAM5-HAM (European Center for Medium-Range Weather
735 Forecasts (ECMWF) and Hamburg) was developed at the Max Planck Institute (MPI) for
736 Meteorology in Hamburg, Germany (Roeckner et al., 2003, 2006; Stier et al., 2005), and adapted
737 to study of aviation effects on climate, including the modeling of the effects from contrails. The
738 aerosol-climate modeling system ECHAM5-HAM is based on a flexible microphysical approach,
739 and it predicts the evolution of an ensemble of microphysically interacting internally and externally
740 mixed aerosol populations as well as their size distribution and composition. Bier and Burkhardt
741 (2022) applied the ECHAM5-HAM model, incorporating a two-moment microphysical scheme
742 that was expanded to introduce a novel cloud category-contrail cirrus. The contrail cirrus scheme
743 encompasses a parameterization addressing contrail ice nucleation, the loss of ice crystals during
744 the vortex phase, plume dilution, the spreading of contrails influenced by vertical wind shear, and
745 inclusive microphysical and macrophysical processes aligned with the natural cloud scheme.

746

747
748
749
750
751
752
753
754
755
756
757
758
759
760
761
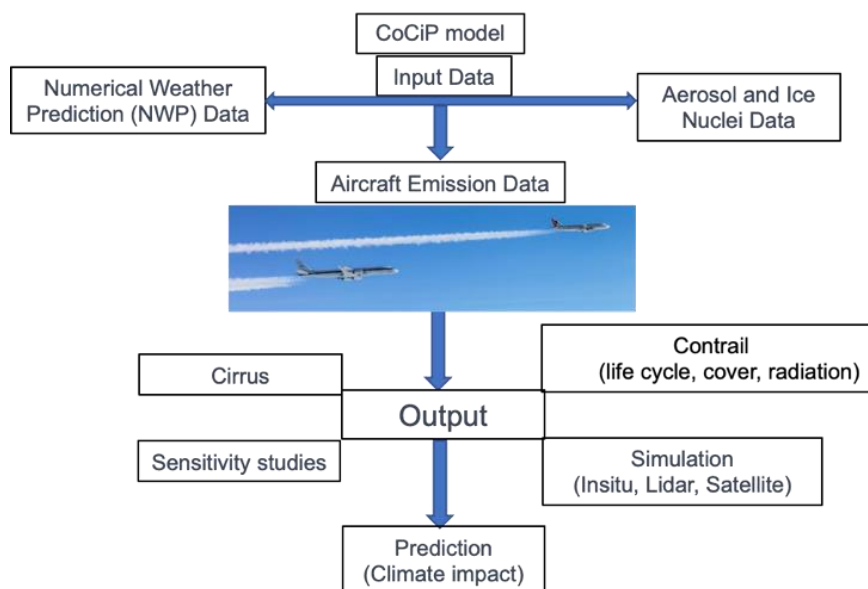
Figure 9. Schematic of the CoCiP model. Adapted from Schumann (2012).

763

764 The contrail cirrus parameterization implemented in ECHAM5-HAM follows the framework
765 established by Burkhardt and Kärcher (2009), who introduced contrail cirrus as a distinct cloud
766 class alongside natural cirrus clouds within the model's natural cloud scheme. The water and heat
767 budgets are balanced, with natural cirrus and contrails competing for available water vapor.
768 Prognostic variables, including ice water content, contrail coverage, and the length of contrail
769 cirrus, are computed based on factors such as persistence, advection, spreading, and
770 deposition/sublimation. Bock and Burkhardt (2016) extended the contrail cirrus parameterization
771 (CCMod) initially proposed by Burkhardt and Kärcher (2009) by incorporating a microphysical
772 two-moment scheme (Lohmann et al., 2008).

773 In this extended parameterization, contrail cirrus ice crystal number concentration and volume are
774 introduced as additional prognostic variables. This enhancement provides a more accurate
775 representation of microphysical processes, proving essential for studies addressing the impact of
776 aircraft particle number emissions on contrail cirrus properties and their overall climate influence.
777 The cloud water content in ECHAM5 typically undergoes growth assuming saturation adjustment.

778 For the initialization of contrail cirrus, a fixed ice crystal number based on observations over
779 Europe was employed (Bock and Burkhardt, 2016). The initialization of contrails occurs at an age
780 of 450 seconds, representing half of a model time step. The incorporated parameterizations and
781 the contrail initialization time are depicted in a simplified scheme presented in Figure 10.

782
783
784
785
786
787
788
789
790
791
792
793
794
795
796
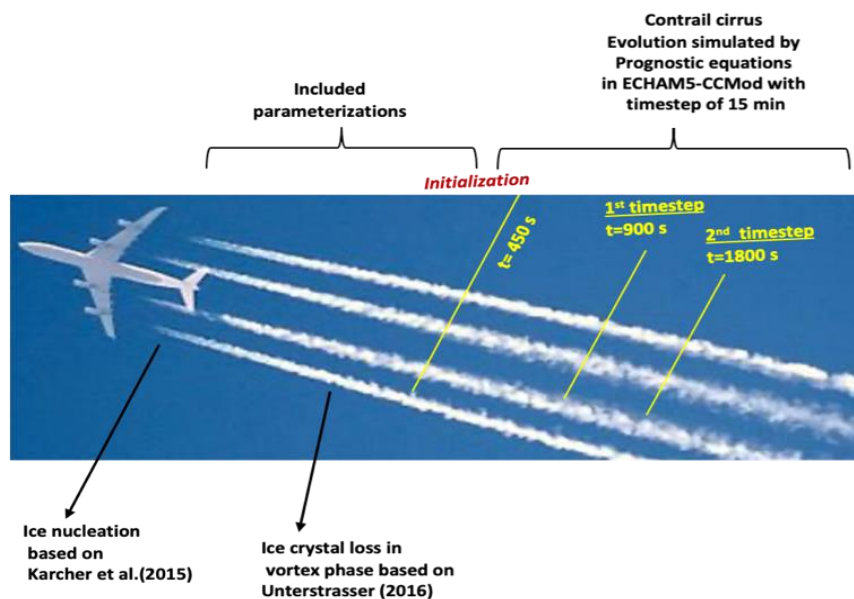
797 **Figure 10.** Stages of contrails and their corresponding treatment into the global climate model
798 ECHAM5-CCMod. Adapted from Bier and Burkhardt (2022).

799 In instances of contrail cirrus volumes exhibiting very low ice crystal number concentrations, as
800 observed in aged contrails associated with heightened ice crystal sedimentation, the deposition of
801 ice water is constrained, aligning with the depositional growth of ice crystals (Bock and Burkhardt,
802 2016). In more recent iterations of the model, specifically ECHAM5-CCMod, Bier and Burkhardt
803 (2019) incorporated the contrail ice nucleation parameterization proposed by Kärcher et al. (2015).
804 In their model approach, they suggest that the plume cools over time due to continuous mixing of
805 the exhaust with ambient air, eventually becoming water-supersaturated when the SAC criterion
806 is met. The number of activated aerosol particles, stemming from soot and ambient particles, is
807 computed based on ambient conditions, fuel/engine characteristics, and exhaust particle properties.
808 Additionally, Bier and Burkhardt (2022) introduced a parameterization for ice crystal loss during
809 the vortex phase and conducted a thorough evaluation of their model

810 **3.2.3 NCAR CAM6 model with Contrails**

811 In the first NCAR study of the radiative forcing of linear contrails and contrail cirrus, Chen and
812 Gettelman (2013) used the Community Atmosphere Model version 5 (CAM5), the atmospheric
813 component of the National Center for Atmospheric Research (NCAR) Community Earth System
814 Model (CESM). More recently, they have used the updated atmospheric component from the new
815 version of CESM2 (Danabasoglu et al., 2020). The current atmospheric model implemented in
816 CESM2 is CAM, version 6.2 (CAM6; Gettelman et al., 2020). CAM6 incorporates a detailed two-
817 moment cloud microphysics scheme (Gettelman and Morrison, 2015) coupled with an aerosol
818 microphysics and chemistry model (Liu et al., 2016; Gettelman et al., 2019). The latest version of
819 the contrail parameterization (Chen et al., 2012) was utilized with CAM6 (Gettelman et al., 2021).
820 While the ice cloud microphysics and aerosols exhibit minimal differences between CAM5 and
821 CAM6, the aerosol activation in CAM6 significantly differs, impacting natural cirrus clouds but
822 not contrails. The assumed emission ice particle diameter was adjusted from the original
823 parameterization (10 µm) to 7.5 µm to better align with observations (e.g., Lee et al., 2021).

824 For contrail studies at NCAR, the standard version of CESM with 32 levels (to 3 hPa) vertical and
825 ~ 1∘ horizontal resolution was employed. Winds and optional temperatures were relaxed to
826 NASA's data assimilation analyses, specifically the Modern-Era Retrospective analysis for
827 Research and Applications, version 2 (MERRA2; et al., 2015), with wind nudging (et al., 2020,
828 2021). CESM2 features a fully interactive land surface model (the Community Land Model,
829 version 5; et al., 2020). Sea surface temperatures (SSTs) are fixed to MERRA2 SST, and there is
830 no interactive ocean.

831 These simulations allow for adjustments in atmospheric and surface temperatures, resulting in
832 radiative flux perturbations representing an Effective Radiative Forcing (ERF). Sensitivity tests
833 were conducted, with temperatures nudged to MERRA2. The results were compared with previous
834 contrail simulations using this model and others, as well as observational data. The pattern of
835 contrail-induced changes to cloud fraction closely resembled the previous model documented in
836 CAM5 (Chen and Gettelman 2013), with peak effects observed in the Northern Hemisphere at
837 mid-latitudes. The radiative forcing in the CAM6 simulations exceeded that of the earlier Chen
838 and Gettelman (2013) study due to a smaller initial contrail area (100 vs. 300 m) and smaller initial
839 ice crystal sizes (7.5 vs. 10 µm diameter). The radiative forcing pattern and magnitude were
840 qualitatively and quantitatively consistent with the analysis conducted by Lee et al. (2021),
841 aligning with the intercomparison between contrail simulation models.

842 3.2.4 Stanford global model for contrail evaluation

843 Although it is no longer actively utilized in aviation studies, Stanford University developed a low-
844 order contrail model and a Large Eddy Simulation (LES) model (Naiman et al., 2009; Naiman et
845 al., 2011; Jacobsen et al., 2011). In their work, Jacobsen et al. (2011) assessed mass-conservative,
846 positive-definite, unconditionally stable, and non-iterative numerical techniques for simulating the
847 evolution of discrete, size, and composition-resolved aerosol and contrail particles within
848 individual aircraft exhaust plumes. This simulation was conducted in a global or regional 3-D
849 atmospheric model, incorporating the coupling of subgrid exhaust plume information to the grid
850 scale (see Fig. 11). This approach represents a distinct method for simulating the impacts of aircraft
851 on climate, contrails, and atmospheric composition.

852 The microphysical processes addressed within each plume include size-resolved coagulation
853 among and between aerosol and contrail particles, aerosol-to-hydrometeor particle ice and liquid
854 nucleation, deposition/sublimation, and condensation/evaporation. Each plume is characterized by

855 its own emission and supersaturation, and the spreading and shearing of each plume's cross-section
856 are calculated over time. Aerosol and contrail-particle core compositions are tracked for each size
857 and affect optical properties within each plume. When linear contrails sublimate or evaporate, their
858 size and composition-resolved aerosol cores and water vapor are introduced to the grid scale,
859 where they influence large-scale clouds. The model's algorithmic properties were analyzed, and
860 the final model was evaluated against in situ and satellite data.

861
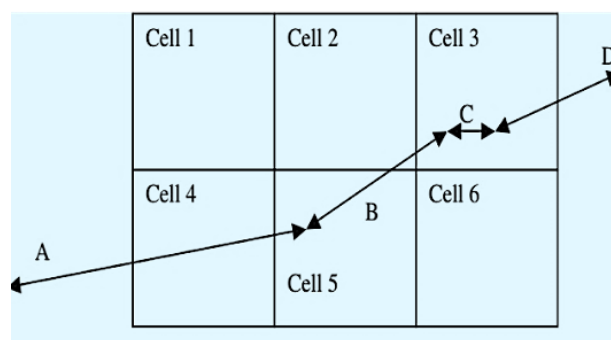
869 **Figure 11.** Example of how flight segments cross grid cell boundaries in the Jacobsen et al., model.
870 Segments A, B, C, and D are original segments. These are partitioned or aggregated into individual
871 model grid cells 2, 3, 4, and 5 to form ''new'' segments. Adapted from Jacobsen et al. (2011).

872

873 **4 Radiative Forcing for Contrail Cirrus in Global Models**

874 **4.1 Contrail radiative forcing and efficacy**

875 Contrails during the day can warm or cool depending on optical depth, zenith angle, and ice crystal
876 shape (Stuber et al. 2006; Newinger and Burkhardt (2012). Stuber et al. (2006) suggested that
877 moving all air traffic to the day decreases RF. Newinger and Burkhardt (2012) stated that we need
878 to consider the lifetime of the contrails since daytime air traffic can cause a large contrail coverage
879 at night. After all, it is the long-lived contrail cirrus outbreaks that are responsible for a large part
880 of the climate impact (Burkhardt et al. 2018). As illustrated in Fig. 1, the overall effect reveals a
881 positive net radiative forcing (RF), signifying a warming impact. The examination of this
882 phenomenon is undertaken here. In contrast to the comprehensive RF, the local RF (RF′) can be
883 defined as the instantaneous change in net incoming radiation for 100% contrail coverage in a
884 specific location.

885 Contrail RF comprises both a long-wave (LW) and a short-wave (SW) component, with each
886 influenced by flight characteristics and the time of day. Unlike the systematic dependency on
887 optical depth (τ), the relationship between RF and ice water path (IWP) is less consistent (De Leon
888 et al., 2012; Schumann et al., 2012). The LW RF is positive both day and night, with the largest
889 impact observed for a cold contrail (located near the tropopause) over a warm, cloud-free Earth
890 surface. The shortwave radiative forcing (RF) is predominantly negative, with the greatest impact
891 observed for contrails over darker surfaces, such as cloud-free oceans (Meerkötter et al., 1999).
892 Studies conducted by Schumann et al. (2012), utilizing both their model and observational
893 evaluations, suggest the existence of substantial regional RF′ values. The calculation of contrail

894   RF within a global model is contingent on factors such as the representation of contrails, the
895   atmospheric conditions, and the radiation transfer model employed (Myhre et al., 2009).

896   Bickel et al. (2020) analyzed the feedback processes and quantified the effective radiative forcing
897   (ERF) of contrail cirrus, which refers to the cloud formations produced by aircraft engine exhaust.
898   They highlighted that feedback analysis is a valuable tool for understanding climate sensitivity and
899   the differences in efficacies between various climate-forcing agents. Previous climate model
900   simulations have suggested a relatively low efficacy of contrails in forcing global mean surface
901   temperature changes. They employed a climate model that incorporates a state-of-the-art
902   representation of contrail cirrus and conducted the simulations with fixed sea surface temperatures
903   to determine the ERF resulting from contrail cirrus.

904   Bickel et al. (2020) noticed that significant scaling up of aviation density is necessary to obtain
905   statistically significant results from the simulations. Their study found that the ERF of contrail
906   cirrus is less than 50% of the respective instantaneous or stratosphere-adjusted radiative forcings.
907   The best estimate of contrail cirrus ERF is approximately 35%. In comparison, the reduction of
908   ERF is more substantial for contrail cirrus than for a similar magnitude increase in CO_2
909   concentrations. They identified the main factor contributing to the reduction in contrail cirrus ERF
910   as a compensating effect of natural clouds that provide negative feedback. Additionally, they
911   observed that the combined water vapor and lapse rate adjustment, which affects the distribution
912   of water vapor in the atmosphere and the lapse rate (temperature decrease with altitude), has a less
913   positive impact on contrail cirrus ERF compared to the reference case of CO_2 forcing.
914   Nevertheless, the negative feedback provided by natural clouds has a more pronounced effect in
915   reducing contrail cirrus ERF compared to these adjustments.

916   Overall, Bickel et al. (2020) suggested that contrail cirrus has a lower climate impact than initially
917   thought, with the reduction in ERF attributed to the compensating effect of natural clouds.
918   Understanding the specific feedback processes and quantifying the ERF of different climate
919   forcing agents, such as contrail cirrus, is crucial for accurately assessing their contributions to
920   surface temperature changes and overall climate dynamics.

921   Long-lasting contrails contribute to global climate change. These contrails can form cirrus clouds,
922   which are a type of high-altitude cloud that can trap heat in the atmosphere. This trapping of heat
923   is known as radiative forcing. While the exact contrail contribution to radiative forcing remains
924   uncertain, it is thought to be a significant factor in climate change (Brasseur et al., 2016). The RF
925   metric is a backward-looking measure of the effect of emissions on the radiative flux balance and
926   is commonly used to compare changes in climate forcings (Wuebbles et al., 2010). The RF linked
927   to non-CO_2 aviation emissions arises from processes occurring over different time scales. Contrails
928   generally exist for a few hours after an aircraft emissions occur, but other emissions can last much
929   longer. Effects on the distribution of aerosols and on ozone produced from NOx emissions can
930   remain for a few days to months, while changes in CH_4 can be affected for longer than a decade.
931   The limitations of using RF as a comprehensive metric for global non-CO_2 aviation climate
932   impacts are well-recognized due to such associated spatiotemporal variations (Wuebbles et al.,
933   2007). The nonlinear interactions involved make it imprecise to represent the sum of RF for various
934   non-CO_2 components as a single value. Similarly, distinct climate responses are observed for
935   different forcing mechanisms.

936   In 2016, Brasseur et al. investigated the radiative forcing (RF) through analyses involving seven
937   global models (CAM4, CAM5, IGSM, GISS-E2, GEOSCCM, GATOR-GCMOM, and GEOS-

CHEM) as part of the Federal Aviation Administration's (FAA) Aviation Climate Change Research Initiative (ACCRI) program. The assessment covered climate impacts for 2006, and the initial five models projected impacts for 2050 scenarios, specifically focusing on selected aircraft emission components. In a separate study, Chen and Gettelman (2016) used the CAM5 model to estimate RF for contrails and contrail cirrus in the 2050 future scenario, employing the 2006 AEDT dataset. Notably, the research highlighted the tendency to overestimate global linear contrail (LC) net RF when using the natural ice cloud optical property parameterization as a stand-in for contrail counterparts in modeling studies. Furthermore, the distribution of regional RF indicated that in densely trafficked airspaces, such as the United States, RF could be up to ten times higher than the global average (Brasseur et al., 2016).

Schumann and Graf (2013) determined a more significant AIC impact by using both observational data and the contrail cirrus prediction model (CoCiP; Schumann, 2012). They found an "aviation fingerprint" ascribed to a daily air traffic cycle within the diurnal cycle of cirrus properties in the North Atlantic region (NAR), associating with the annual mean diurnal patterns of cirrus cover and outgoing longwave radiation (OLR) derived from Meteosat data (Graf et al., 2012).

Figure 12 shows the global average annual radiative forcing (RF) values and uncertainty ranges for persistent contrails alone and together with contrail cirrus. The values are compiled from selected studies and assessments published since 1999 and include a recent development by Kärcher (2018). Over time, early assessments of contrail RF have been confirmed and the range of uncertainty has been narrowed down considerably.
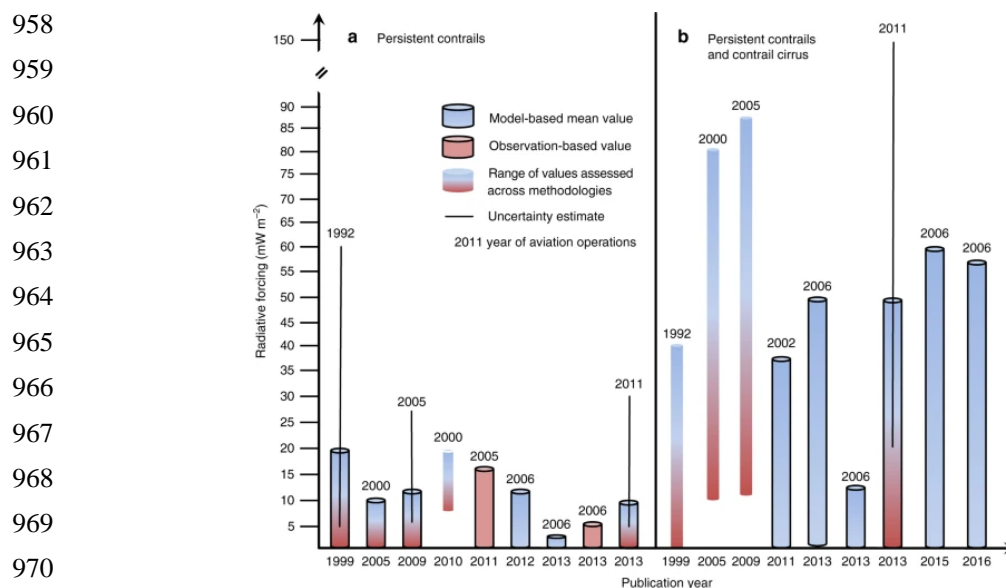
Figure 12. Global annual average amount of radiative forcing caused by aircraft-induced clouds Figure adapted with permission from Kärcher (2018). (Licensed under CC BY 4.0)

The figure shows that the RF due to persistent contrails alone is -0.01 W/m² (with an uncertainty range of 0.005-0.03 W/m²), and the RF due to persistent contrails together with contrail cirrus is ~0.05 W/m² (with an uncertainty range of 0.02-0.15 W/m²). (Kärcher, 2018). Figure. 12 shows

977 that analyses accounting only for linear contrails underestimate the total RF for contrails. More
978 recent analyses tend to show an overall warming of around ~45mWm^{-2} (Bier and Burkhardt, 2022).

979 The models applied by DLR and NCAR's groups are summarized in Table 2 (updated from. Bock
980 and Burkhardt, 2016). Bock and Burkhardt (2016) evaluated the year 2002 using the AERO2k
981 inventory and for year 2006 using the AEDT 2006 slant distance inventory. The corrected NCAR
982 analyses and their more recent results are consistent with those from the DLR modeling studies
983 (Lee et al., 2021). These findings further amplify the conclusions from Fig. 12.

984 **4.2 Future RF projections**

985 **4.2.1 DLR's study for future RF projections**

986 Bock and Burkhardt (2019) investigated how changes in air traffic between 2006 and 2050 would
987 impact the properties of contrail cirrus clouds and the amount of radiative forcing they exert. They
988 considered both the increase in air traffic volume and the upward shift in flight altitudes. As shown
989 in Table 3, air traffic is projected to increase fourfold, while flight altitudes are expected to rise by
990 0.3 to 1.5 km. This shift will result in the maximum flight density occurring at a lower altitude,
991 around 200 hPa in 2050 compared to 240 hPa in 2006. They found that the maximum flight density
992 would occur at a lower altitude in 2050, which would have implications for the climate (Bock and
993 Burkhardt, 2019).

994 **Table 2.** Summary of existing contrail cirrus simulations and RF from the DLR and NCAR
995 models. Adapted from of Bock and Burkhardt (2016).
996

Model	Inventory	Flight distance	RF (mW/m^2)	References
ECHAM5-CCMod	AERO2k 2002	track	35	
ECHAM5-CCMod	AEDT 2006	track	49	*Burkhardt and Kärcher* (2011)
ECHAM5-CCMod	AEDT 2006	slant	56	
ECHAM4-CCMod	AERO2k 2002	track	38	
ECHAM4-CCMod	REACT4C 2006	track	45	*Schumann et al,* (2015)
COCIP	AEDT 2006	flight vectors	63	*Schumann et al.* (2015)
CAM5	AEDT 2006	slant	13 (57)*	*Chen and Gettelman* (2013)
CAM6	AEDT 2006	slant	62 (ERF)**	*Gettelman et al.* (2021)

* The approximation of Chen and Gettelman (2013) was revised.

**ERF (the scaling technique was derived from Lee et al.2021 for 2006 to 2018 and then 9% per year scaled (2018 to 2019)
by Gettelman et al. (2021)

997

998 In Table 3, the air traffic distance is specified as the ground-projected track distance. The coverage
999 is sketched out for all contrail cirrus, and the visibility of contrail cirrus (visible optical depth >
1000 0.05) is indicated in brackets (Bock and Burkhardt, 2016). Radiative forcing estimates exist for
1001 both track distance and slant distance within brackets (Table 3). Remarkably, Bock and Burkhardt
1002 (2019) determined that the projected future increase in air traffic, coupled with a minor shift to
1003 higher altitudes, outcomes in a substantial rise in contrail cirrus coverage, optical depth, and
1004 radiative forcing. Particularly, air traffic contrail cirrus radiative forcing is estimated to increase
1005 threefold, from 49 to 159 mW m^{-2} (Fig. 13). The findings are a result of a future air traffic
1006 inventory, where the measurement of air traffic is signified in terms of track distance (ground
1007 projected) rather than slant distance (3-D). Declining the initial contrail ice particle number by

1008   50% results in a substantial drop in the climate impact of contrail cirrus, leading to a global decline
1009   in radiative forcing for the year 2050. The reduction is significant, amounting to a 14% reduction
1010   from 160 to 137 mWm−2. (Fig. 13).

1011 4.2.2 RF projections from the NCAR model

1012   The study conducted by Chen and Gettelman (2016) investigated the radiative forcing curbing
1013   from aviation-induced cloudiness, using the Community Atmosphere Model Version 5 (CAM5)
1014   for both present (2006) and future (up to 2050) scenarios. The researchers found a projected four-
1015   fold increase in global flight distance from 2006 to 2050. In spite of this, the simulated radiative
1016   forcing from contrail cirrus in 2050 is predicted to reach 87 mWm^{-2}, representing a seven-fold
1017   rise compared to 2006. This underlines a non-linear correlation between radiative forcing and fuel
1018   emission mass, accredited to non-uniform regional escalations in air traffic and changes in contrail
1019   radiative forcing sensitivity through different regions.

1020   **Table 3.** Overview of the model simulations: Air traffic distance exists as ground-projected track
1021   distance. Coverage is furnished for all contrail cirrus, with coverage for visible contrail cirrus
1022   (visible optical depth > 0.05) shown in brackets (Bock and Burkhardt, 2016). The radiative
1023   forcing is represented for both track distance and slant distance, with values enclosed in brackets.
1024   (Adapted from Bock and Burkhardt (2019)

Background	Inventory	Air traffic volume (km yr^{-1})	Propulsion efficiency	Initial ice number concentration (cm^{-3})	Coverage (%)	RF (mW m^{-2})
2006	2006	3.7×10^{10}	0.3	150	1.1 (0.7)	49 (56)
2006	2050 Baseline	15.4×10^{10}	0.3	150	2.9 (2.0)	159 (182*)
2050 (RCP6)	2050 Baseline	15.4×10^{10}	0.3	150	2.8 (2.0)	160 (183*)
2050 (RCP6)	2050 Scenario1	15.4×10^{10}	0.42	75	2.98(1.7)	137 (157*)

RCP6-Representative Concentration Pathway 6.0

*Asterisks denote extrapolated values resultant from the factor resolute by the radiative forcing in 2006, which is connected
to air traffic volume and computed using slant distance and track distance (Bock and Burkhardt, 2016).

1025   The CAM5 simulations also indicate that the negative radiative forcing resulting from the indirect
1026   effect of aviation sulfate aerosols on liquid clouds in 2050 could be as large as -160 mWm^{-2}, a
1027   four-fold increase from 2006. Consequently, when considering both aviation aerosols and contrail
1028   cirrus, the total radiative forcing in 2050 could possibly employ a cooling impact on the planet.
1029   Aerosols, particularly aviation sulfate aerosols distributed at cruise altitudes, may be transferred
1030   to the lower troposphere. This procedure raises aerosol concentrations and consequently enhances
1031   the cloud drop number concentration and persistence of low-level clouds. On the other hand, the
1032   study suggests that aviation black carbon aerosols have an insignificant net forcing affect globally,
1033   both in 2006 and 2050.

1034   The researchers focus on specific regions, for instance, Central Europe, eastern North America,
1035   and East Asia, and recommend quantitative evaluations of the forcing in each region for several
1036   scenarios. For example, in Central Europe, the predicted contrail cirrus radiative forcing in 2050
1037   is anticipated to locally peak at 2 Wm^{-2}, marking a 2 to 3-fold increase compared to 2006. In the
1038   eastern United States, the contrail cirrus radiative forcing could reach 800 mWm−2 in 2050,

revealing a higher percentage increase compared to 2006. The most prominent rise in contrail cirrus radiative forcing is estimated in East Asia, where a 6-fold increase is projected for 2050, associated with the region's anticipated significant rise in consumption of aviation fuel Inclusion of aviation aerosols in the simulations suggests a slight reduction in positive forcing over land, as compared to the forcing solely caused by contrail cirrus. On the other hand, over the ocean, a negative forcing rising from aviation emissions is measured. This can be accredited to the lower surface albedo and cleaner environment (fewer aerosols) in comparison to land areas. In the three regions with the highest projected air traffic in 2050 (eastern United States, Central Europe, and East Asia), aviation aerosols reduce the regionally averaged positive radiative forcing induced by contrail cirrus by approximately 50%, as indicated by the blue boxes in Fig. 14. The peak positive forcing within each of these regions is also reduced by 50% due to aviation aerosols. The study provides detailed regional estimates of these effects (Table 4).

The negative radiative forcing result from aviation aerosols, as detected in this study, supports with the inferences represented by Righi et al. (2013). The extent of the cooling effect is estimated to be affected by the background cloud drop number concentration.
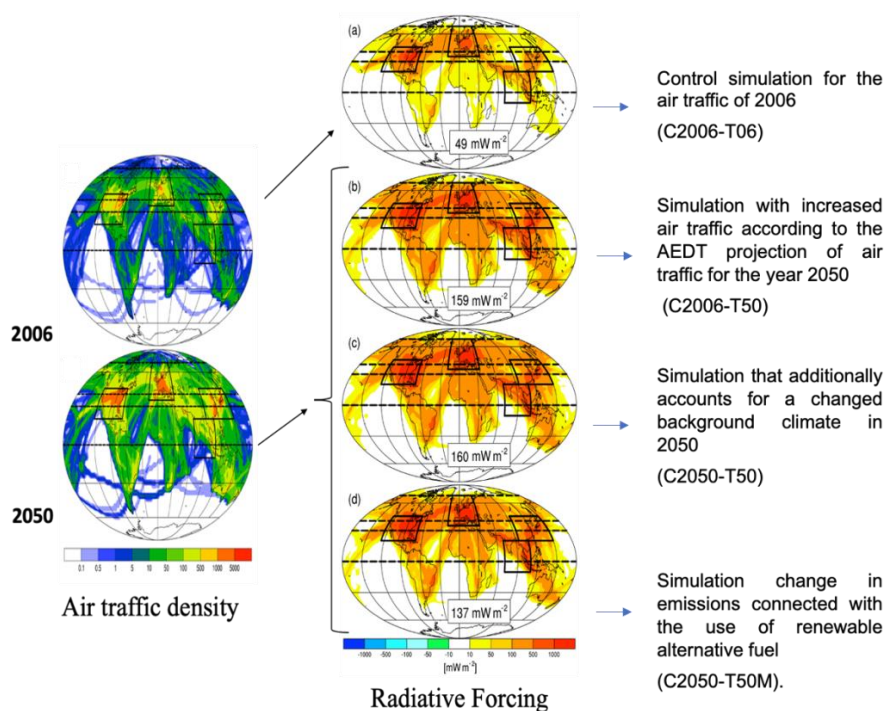
Figure 13. The horizontal distribution depicts the vertically incorporated air traffic density (km $m^{-2}s^{-1}$) for the years 2006 and 2050, along with the radiative forcing in scenarios C2006-T06 (a), C2006-T50 (b), C2050-T50 (c), and C2050-T50M (d) Adapted from Bock and Burkhardt (2019).

Table 4. Radiative forcing (mWm^{-2}) attributed to aviation H_2O emissions, with uncertainties derived from 2 standard deviations of the four-member ensemble. (Adapted from Chen and Gettelman, 2016)

Meteorology	Scenario	Global	North America	Central Europe	East Asia
Present	2006 AIR	12 ± 4	195 ± 30	483 ± 69	41± 8
2050 RCP4.5	2050 BL	87 ± 6	798 ±152	1682 ± 535	272 ± 39
2050 RCP4.5	2050 SC1	76 ± 7	724 ± 136	1568 ± 489	231 ± 36
2050 RCP4.5	2050 SC2	76 ± 7	724 ± 136	1568 ± 489	231 ± 36
2050 RCP4.5	2050 SC3	80	681	1952	213
2050 RCP8.5	2050 BL	83 ± 3	852 ± 92	1558 ± 226	248 ± 25
2050 RCP8.5	2050 SC1	73 ± 4	777 ± 96	1442 ±235	211 ± 24
2050 RCP8.5	2050 SC2	73 ± 4	777 ± 96	1442 ±235	211 ± 24
2050 RCP8.5	2050 SC3	75	865	1597	221

1077
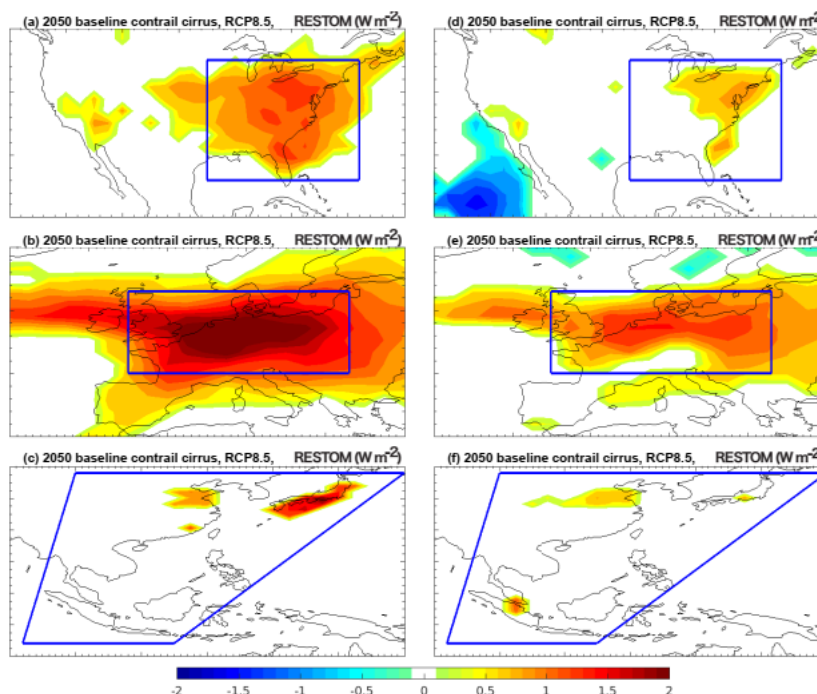
1078

Figure 14. Ensemble of the average regional radiative forcing in Wm−2, utilizing the baseline emission scenario for the year 2050 with RCP8.5 meteorology, focusing on contrail cirrus alone (a–c) and contrail cirrus combined with aviation aerosols (d–f). The term "RESTOM" represents the alteration in the net residual radiative flux at the top of the model. The plot includes only ensemble-mean perturbations that surpass 2 standard deviations of the averaged control simulations. (Figure adopted with permission from Chen and Gettelman, 2016) (Licensed under CC BY 4.0)

1086   **4.3 Issues representing cloud-contrail and contrail-contrail overlaps in modeling studies**

1087   A thorough examination of past methodologies for modeling cloud layer overlaps and several
1088   modeling studies recommends that overlapping with other cloud layers is prone to reduce both the
1089   shortwave (cooling) and longwave (warming) radiative forcing linked to contrails (Sanz-Morère
1090   et al., 2021). However, there is inadequate agreement on how the overlap between clouds and
1091   contrails might modify the net radiative forcing due to uncertainties regarding whether it would
1092   more strongly mitigate the shortwave or longwave components. Particularly, the precise impact of
1093   contrail-contrail overlap on global contrail radiative forcing has yet to be measured. In this section,
1094   we review previous literature referring to the treatment of multiple-layer overlap in the context of
1095   contrail radiative forcing calculations.

1096   Schumann et al. (2012) determined that the net radiative forcing may augment if contrails overlap
1097   with low-level clouds but could go through significant variations when passing under natural cirrus
1098   clouds. This underscores the significance of precisely modeling natural clouds in contrail
1099   simulations. Nevertheless, when utilizing this method to simulate single contrails, accounting for
1100   the radiative interactions among multiple contrails turns into a challenging task. In prior examples
1101   of modeling contrail-contrail overlap, when simulating contrails in global climate models, various
1102   treatments have been utilized, as outlined in Table 5. Contrail parametrizations have been
1103   formulated for ECHAM4 (Ponater et al., 2002; Burkhardt and Kärcher, 2009), where maximum-
1104   random overlap is presumed between contrail and cloud layers, as well as among different contrails
1105   (Burkhardt and Kärcher, 2011; Marquart et al., 2003; Bock and Burkhardt, 2016; Frömming et al.,
1106   2011). Rädel and Shine (2008) and Rap et al. (2010) also use this parameterization, calibrating
1107   the outcomes by using satellite observations.

1108

1109   **Table 5.** Existing methods for modeling contrail–contrail overlap when estimating global contrail
1110   RF. MRO: maximum-random overlap, defined by Geleyn and Hollingsworth (1978) as assuming
1111   that clouds in adjacent layers maximally overlap, while clouds separated by one or more clear
1112   layers randomly overlap (Adapted from Sanz-Morère et al. 2021).

Source	Model used to represent contrail–contrail overlap
Minnis et al. (1999)	No overlap considered (fractional coverage from observations)
Marquart et al. (2003)	MRO in the vertical for each column
Rädel and Shine (2008)	Random overlap
Rap et al. (2010)	Random overlap
Frömming et al. (2011)	MRO in the vertical for each column
Burkhardt and Kärcher (2011)	MRO in the vertical for each column
Chen and Gettelman (2013)	Zero contrail–contrail overlap in grid box
Schumann and Graf. (2013)	Linear RF addition
Bock and Burkhardt (2016)	MRO in the vertical for each column

1113

1114   Chen and Gettelman (2013) included contrails in the CAM5 model by portraying them as an
1115   increase in the 3-D cloud fraction, where the model presumes maximum-random overlap.
1116   Nevertheless, in their method, they considered zero overlaps between newly formed contrails when
1117   placed at the same vertical level (approximately 1 km).Finally, the CoCiP Lagrangian contrail
1118   model (Schumann, 2012) reports contrail-contrail overlaps indirectly by linearly summing the

radiative forcing of all contrails, taking into consideration any observed cirrus present above the simulated contrail.. Nonetheless, this method does not clearly consider the overlap between simulated contrails. Inconsistencies rise in how contrail-contrail overlaps are modeled across various studies. The most efficient approach remains uncertain, and as of now, no analysis has measured the impact of contrail-contrail overlaps on global contrail RF. Since further expansion of the aviation sector is expected, it is anticipated that an increased number of instances of contrail overlap will occur. Hence, a more inclusive understanding of the degree and dynamics of contrail-contrail overlap is a necessity.

5 Observation Datasets for Contrail Studies

The vast majority of observations, comprised of airborne, satellite, and ground-based approaches, encompass jet aircraft exhaust contrails from 1972 onward. Nevertheless, it is remarkable that records of contrail observations date back to as early as 1915, as observed by Ettenreich in 1919.

Early measurements performed behind a propeller-driven aircraft offered data supporting the concept that contrail ice formation requires liquid saturation to originate, associating with the Schmidt-Appleman criterion that is now well-established (aufm Kampe, 1943; Schumann, 1996). These remarks, which encompassed the collection of ice particles on impactors and halo observations, also furnished initial insights into the size and shape of both contrail and cirrus ice particles (Weickmann, 1945). The precise testing of models necessitates reliable quantitative data, covering not only information on contrail and plume properties but also on contrail age, the generating aircraft, atmospheric conditions during contrail formation, and the observational methods employed (Schumann et al., 2017). Mean properties of individual contrails are characterized for a wide range of jet aircraft as a function of age during their life cycle from seconds to 11.5 h (7.4-18.7 km altitude, -88 to -31℃ ambient temperature), based on a compilation of about 230 in-situ and remote sensing measurements (Schumann et al., 2017). Contrails from individual aircraft can remain visible for extended periods, as reported in analyses by Minnis et al. 1998 and Minnis et al. 2013) and Vázquez-Navarro et al. (2015). Schumann et al. (2017) furnished a brief description of individual datasets, integrating new analyses for their study, and combined them to create a "contrail library" (COLI). This dataset was then compared with the outcomes of the Contrail Cirrus Prediction (CoCiP) model. The observations corroborate that the quantity of ice particles in contrails is controlled by both the engine exhaust and the formation process in the jet phase. Some particle losses ensue in the wake vortex phase, with succeeding gradual diminishes over time.

Publicly available air traffic data are usually limited, but certain projects have gathered flight data from sources such as air traffic control or ground-based observations (Schumann et al., 2013; Schumann et al., 2016). Distinguishable projects with air traffic subsets since 2005 are accredited. Garber et al. (2005) compiled traffic data for the United States and southern Canada for the years 2000-2005. In Germany, the Deutsche Flugsicherung (DFS) has been gathering and filing away traffic data from 2006 onwards for more new projects. The Aviation and Climate Change Research Initiative (ACCRI; Brasseur et al., 2016) furnished a global waypoint dataset for the year 2006 to researchers included in the ACCRI project.

Particulars about aircraft assets, including size, mass, speed, fuel consumption, and propulsion efficiency, were tracked from various references, including the BADA (EUROCONTROL, 2009). Added engine properties, such as fuel consumption and emissions at surface pressure, can be

1162   attained from the ICAO Aircraft Engine Emissions Databank (EASA, 2023) and the 2006 AEDT
1163   emissions inventory (Barrett, 2010; Wilkerson, 2010)

1164   Two sets of observational-based capabilities exist that can provide the coverage needed to help
1165   evaluate the global modeling analyses for treating the effects of contrails, the Contrail Library
1166   (COLI) and the satellite-based record. The Contrail Library results are useful for evaluating limited
1167   areas of contrails but not for global analyses.

5.1 Contrail Library (COLI)

1169   The COLI database includes 236 entries describing properties of contrails with known ages,
1170   including mean data for one hundred cases of in-situ measurements, more than 70 cases from
1171   ground-based and airborne lidar observations, 50 cases from satellites, and a few camera
1172   observations. The data come from 33 observation projects during the last 45 years. The comparison
1173   of the data from various measurements shows notable differences among the various instruments
1174   utilized across the dataset. Nevertheless, a notable accord endures among each approach, as well
1175   as uniformity between in-situ and remote sensing results, along with agreement with Schumann et
1176   al (2017) model outcomes. Moreover, in-situ data resultant from contrail measurements, the
1177   investigation integrates remote sensing data found from ground-based or airborne lidar and
1178   spectroradiometer, satellites, cameras, and visual interpretations. Table 6 summarizes some of the
1179   projects that contributed to the COLI database, including the aircraft used and the primary location,
1180   the mode of reference and a primary reference of the study.

5.2 Satellite-based datasets

1182   Over the past two decades, detection of contrail in satellite imagery has primarily depended on the
1183   algorithm developed by Mannstein et al. (2003) (e.g., Palikonda et al., 2005; Vazquez-Navarro et
1184   al., 2010). This algorithm contains a series of convolution and thresholding operations related to
1185   brightness temperature images and, subsequently the detection of linear associated components of
1186   fitting size. While the algorithm has been fine-tuned to attain either high precision or high
1187   remembrance in contrail detections, no single model has simultaneously surpassed in both aspects.
1188   Subsequently, empirical observations of contrail coverage often need broad lower-bound/upper-
1189   bound approaches (Duda et al., 2013). Minnis et al. (2013) reported the properties of contrail cirrus
1190   clouds formed during 11 different contrail outbreaks, in the context of objectively determined
1191   linear contrails and their properties. It was observed that the ratio of contrail cirrus to linear
1192   contrails is substantially affected by the satellite analysis algorithm utilized to allocate linear
1193   contrails. Furthermore, this ratio seems to be affected by the presence of overlapping contrails,
1194   which can obscure individual contrails.

1195   The contrail cirrus optical depths were found to be 2-3 times greater than their linear contrail
1196   counterparts and the associated ice crystal particle diameters were 20% greater than the contrail
1197   particle sizes. The analyses of such satellite datasets are likely to be useful for evaluating global
1198   models of contrail radiative effects.

1199   An exception to the application of the Mannstein et al. (2013) algorithm is prominent in Kulik
1200   (2019) and Meijer et al. (2021). These analyses employed a deep learning model for pixel-level
1201   contrail detection using GOES-16 satellite imagery. Upon detecting a contrail, these studies
1202   facilitate the assessment of its lifetime impact and the ascription of potentially relevant flights
1203   (Vazquez-Navarro et al., 2010; Vazquez-Navarro et al., 2013; Vazquez-Navarro et al., 2015.
1204   Mutually, these practices furnish a means to evaluate the efficacy of flight diversions in avoiding

1205 contrail formations. McCloskey et al. (2021) officially released the first large dataset of pixel-level
1206 contrail locations in Landsat-8 satellite imagery labeled by humans. Labelers should be able to
1207 accurately differentiate contrails from naturally occurring cirrus due to Landsat-8's high spatial
1208 resolution and the advected flight history information provided. This dataset will be useful in
1209 benchmarking contrail detection models and validating contrail research in collocated
1210 geostationary satellite imagery.

1211

1212 **Table 6.** Observations from the year 2000 to 2014 incorporated into the COLI for the study of
1213 contrail (Adapted from Schumann et al. 2016).

Year	Project name	Source aircraft	Carrier/location	Measurement	Reference
2000	Cluster	airliners	Great Lakes	satellite	Duda et al.,(2004)
2001	Shutdown	B747+C fighters	Northwestern USA	satellites	Minnis et al.,(2002)
2002	CRYSTAL-FACE	WB-57	NASA WB-57	in situ	Gao et al.,(2006)
2003	Fallstreaks 2003	airliners	Goddard	lidar	Atlas and Wang (2010)
2005	PAZI-2	airliners	DLR Falcon	in situ	Febvre et al.,(2009)
2006	CR-AVE	WB-57	NASA WB-57	in situ	Flores et al.,(2006)
2008	CONCERT	airliners	DLR Falcon	in situ	Voigt et al.,(2010)
2008	ACTA	airliners	Europe andNorth Atlantic	satellite	Vázquez-Navarro et al.,(2015)
2011	CONCERT2011	airliners	DLR Falcon	in situ	Kaufmann et al.,(2014)
2011	COSIC	Bae 146	FAAM Bae-146	in situ	Jones et al.,(2012)
2012	Cameras	airliners	Munich	cameras	Schumann et al.,(2013)
2014	ML-CIRRUS	B772 or F900	HALO	in situ	Voigt et al.,(2016)

1214

1215 Ng et al. (2023) presented a human-labeled dataset named open contrails to train and evaluate
1216 contrail detection models based on GOES-16 Advanced Baseline Imager (ABI) data. Ng et al.
1217 (2023) proposed and evaluated a contrail detection model that incorporates temporal context for
1218 improved detection accuracy. The human-labeled dataset and the contrail detection outputs are
1219 publicly available on Google Cloud Storage at gs://goes_contrails_dataset.

1220 Persuading policymakers and airlines about the climate benefits of flight diversions becomes more
1221 reasonable with the availability of satellite corroboration capabilities. Geostationary satellites like
1222 GOES-16 and low-earth orbit satellites such as Landsat-8 present both complementary strengths
1223 and weaknesses when employed for the task of contrail detection (i.e., coverage versus persistence
1224 of the observations). An automated contrail detection system is essential for developing and
1225 evaluating contrail avoidance systems. Deep neural networks can be employed as an automated
1226 contrail detection system, a form of artificial intelligence (AI) and machine learning (ML), that
1227 has been advanced to connect and categorize contrails in satellite imagery or other relevant data
1228 sources. This system can effectively analyze complex patterns and features associated with
1229 contrails, by leveraging the competencies of deep neural networks. By utilizing deep neural
1230 networks and machine learning techniques, the automated contrail detection system offers an
1231 efficient and reliable solution for detecting and monitoring contrails, facilitating further research
1232 and analysis of their impact on climate and aviation.

1233 Siddiqui (2020) conducted a study where a neural network was used to distinguish contrail cirrus
1234 clouds from regular cirrus clouds on TSI images. The study found that the neural network
1235 triumphed with a high accuracy of 98.5% on the validation set, implying that the model was able
1236 to learn significant visual features of contrails that differentiate them from regular cirrus clouds.

1237 The success of this model opens various practical applications for studying contrails. For instance,
1238 the model can be used to analyze images from different months of data, agreeing for researchers
1239 to investigate the frequencies of contrail occurrences. This can impart valuable insights into air
1240 traffic trends, as well as how physical conditions like temperature and humidity vary seasonally
1241 and their potential impact on contrail formation. Researchers can better understand contrail
1242 behavior and their relationship with various environmental factors by leveraging the neural
1243 network's ability to detect and classify contrails accurately. This knowledge can be used to refine
1244 models and predictions related to contrail formation and persistence and contribute to a more
1245 comprehensive understanding of aviation's impact on the atmosphere.

1246 6 Supersonic contrails

1247 Contrail studies have primarily focused on subsonic aviation due to the predominance of subsonic
1248 air traffic since the retirement of the Concorde in 2003. Contrail formation and persistence for
1249 supersonic commercial aircraft pose challenges -- persistent contrails are unlikely to form in the
1250 stratosphere when these aircraft are flying at supersonic speeds but societal requirements for flying
1251 at subsonic speeds over land to avoid noise issues would still potentially produce persistent
1252 contrails. Limited literature exists, and uncertainties persist regarding parameters controlling
1253 contrail ice crystal distribution evolution for these aircraft. Consequently, the presence or absence
1254 of contrails becomes a discernible marker of the aircraft's speed regime.

1255 7 Uncertainties and Research Gaps

1256 7.1 Uncertainties

1257 There are several crucial areas of uncertainty and research gaps that require focused investigation
1258 to achieve a more comprehensive understanding of contrail formation, evolution, and their effects:

1259 • *Humidity Observations and Predictions:* An important uncertainty lies in the accuracy and
1260 reliability of humidity observations and predictions at different altitudes. Improved
1261 measurements and modeling of humidity are critical for assessing the conditions conducive to
1262 persistent contrail formation and their subsequent behavior. Addressing this uncertainty will
1263 lead to more precise insights into contrail persistence and its associated radiative impacts.

1264 • *Aircraft Plume Mixing:* Uncertainty persists in referring to how ambient air mixes with the
1265 aircraft plume during contrail formation, comprising uncertainties associated with the rate and
1266 extent of mixing.

1267 • *Interaction with Natural Cirrus Clouds:* The interplay between natural cirrus clouds and
1268 contrails initiates an additional level of uncertainty, fostering obscuring the understanding of
1269 their individual and mutual effects on radiative forcing (RF).

1270 • *Regional Variations in Atmospheric Conditions:* The sensitivity of contrail radiative impacts
1271 to regional variations in atmospheric conditions is not well understood and remains uncertain.

1272 • *Aerosols and Aircraft Emissions:* Uncertainties persist in understanding the role of aerosols
1273 and particles from aircraft emissions in contrail formation and properties.

1274

1275 Significant uncertainties persist regarding the radiative forcing caused by aircraft contrails. These
1276 uncertainties arise from numerous factors, starting with uncertainties in the background
1277 meteorology and specific aircraft emissions. When assessing the climate impact of contrail cirrus,
1278 the primary uncertainties lie in (1) determining upper tropospheric water vapor concentrations and
1279 regions of supersaturation; (2) adequately representing contrail cirrus processes in global models;

and (3) understanding the radiative response resulting from the contrail cirrus presence, typically, only approximate assessments of uncertainties associated with these processes are furnished.

Assessing the radiative response of contrail cirrus involves handling several crucial uncertainties, including:

- *Radiative Transfer Scheme:* Uncertainties exist in the radiative transfer scheme employed in the models, accounting for roughly 35% of the overall uncertainty (Myhre et al., 2009).
- *Cloud Heterogeneity:* Uncertainties arise associated with the heterogeneity of ice clouds within the grid box of a climate model (Carlin et al., 2002; Pomroy and Illingworth, 2000), vertical cloud overlap, and the implementation of plane-parallel geometry instead of full 3D radiative transfer (Gounou and Hogan, 2007).
- *Ice Crystal Habit:* Variations in ice crystal habit account for approximately 20% of the overall uncertainty (according to Markowicz and Witek, 2011). Evaluations of radiative transfer treatments within a global climate model, mainly in the context of very small ice crystals in young contrails, reveal uncertainties of up to 10% (Bock and Burkhardt, 2016). The degree of this uncertainty is dependent upon the ice water content of contrail cirrus.
- *Soot Cores:* Radiative transfer uncertainties arise from the presence of soot cores within ice crystals of contrail cirrus, affecting factors such as shortwave albedo (Liou et al., 2013). When reflecting the distinct nature of various uncertainties and eliminating the influence of soot cores in ice crystals, the total uncertainty in the radiative response to contrail cirrus is valued to be around 55%.
- *Upper Tropospheric Water Budget:* Additionally, uncertainties in contrail cirrus radiative forcing (RF) are associated with the upper-tropospheric water budget and the contrail cirrus pattern, including:
  - Uncertainties in contrail cirrus RF are associated with upper-tropospheric ice supersaturation, reducing from the limited vertical resolution of satellite instruments (Lamquin et al., 2012) and contests in reproducing observed statistics of ice supersaturation in current models. This contributes approximately 20% to the total uncertainty.
  - Uncertainties also arise concerning ice crystal number densities within young contrails. Lee et al. (2021) presumed a 50% uncertainty in average contrail ice crystal numbers after the vortex phase, causing an uncertainty of around 20% in contrail cirrus RF. This hypothesis is justified in simulations with ECHAM5-CCMod (Burkhardt et al., 2018).
  - The effect of the lifetime of contrail cirrus on assessed contrail cirrus RF is relatively lesser, affecting day-night contrail cover (Chen and Gettelman, 2013; Newinger and Burkhardt, 2012). The related uncertainty is valued at 5-10% (Lee et al., 2021).
  - The estimation of RF by Chen and Gettelman (2013) faces uncertainties associated with postulations about initial ice crystal radii and contrail cross-sectional areas, accounting for approximately 33% uncertainty.
  - Overall, substantial uncertainties persist in the radiative forcing induced by aircraft contrails, particularly following their transformation into cirrus clouds.

In summary, there are numerous complexities and uncertainties associated with the radiative impacts of aircraft contrails and contrail cirrus clouds. Addressing these uncertainties through improved observations, modeling, and research is crucial for obtaining a more accurate understanding of their role in climate change.

7.2 Research needs and gaps

In the pursuit of a comprehensive understanding of contrail impacts on climate, there is a critical need to establish clear research needs and requirements.

Improving weather models demands better predictions of humidity and clouds with enhanced resolution in time, space, and altitude. The models must also adapt to evolving weather conditions. Accurate water vapor data during cruise altitudes is crucial, emphasizing the need for small, cost-effective humidity sensors. To achieve this, there is a need for the production, testing, and evaluation of precise sensors. Lidar technology and weather model assessments play a key role in advancing observational capabilities for more accurate predictions. Enhancing cirrus cloud forecasts requires a dual focus on data and artificial intelligence. Ensemble simulations are vital for estimating uncertainties in cirrus cloud predictions. Additionally, there is an urgent need for more climate and contrail models, ensuring a comprehensive understanding and evaluation of these complex atmospheric processes.

Sun and Roosenbrand (2023) reported the limitations in traditional computer vision approaches for contrail detection, particularly in handling the complexity of satellite images under varying conditions. Earlier machine learning methods relied on simpler convolutional neural network models, primarily demanding extensive labeled data for contrail presence determination. Notably, there is a gap in the existing literature, lacking research specifically tailored to machine learning approaches for contrail detection, setting it apart from other image segmentation or detection tasks. A significant challenge lies in the absence of adequate loss functions optimized for linear features like contrails during training, making detection notably difficult at lower resolutions, especially when multiple contrails are close. Addressing these gaps is crucial for advancing the efficacy of contrail detection methods (Sun and Roosenbrand, 2023).

Additional research is needed before contrail effects on climate are fully understood. Here are some of the key areas of research gaps that should be explored to address existing uncertainties:

- *Properties of Contrail Particles*: Understanding contrail effects on climate requires reflection of key factors such as particle size, layer height, cloud overlap, and optical properties. Larger particles tend to have a different radiative impact than smaller ones. The altitude of contrail formation impacts their interaction with solar and terrestrial radiation. Precise climate modeling requires proper accounting for cloud overlap, impacting radiative calculations. Contrail optical properties, comprising albedo and emissivity, determine their reflective and trapping abilities for solar and terrestrial radiation. The concentration and size distribution of contrail particles affect their formation and radiative impact. Accurate estimation of contrail forcing, important for climate modeling and policy decisions, depends on understanding particle number, size, and layer height.
- *Assessment of Effective Radiative Forcing:* ERF calculates the radiative impact of contrail cirrus on climate, dependent on comprehending rapid feedback mechanisms. Contrail cirrus can instigate feedback mechanisms affecting their behavior and radiative effects. An advanced understanding of these mechanisms develops the representation of contrail cirrus in climate models, thereby augmenting the accuracy of climate change analyses.
- *Emissions and Alternative Fuels*: Corroborating a precise connection between soot and contrail ice crystal numbers is important for understanding the environmental impact of sustainable aviation fuels, such as biofuels. Biofuels are being studied as a more sustainable alternative to conventional aviation fuels, and evaluating their impact on contrail formation

is crucial for assessing environmental benefits. Scientific research, notifying regulatory decisions, relies on the interpretation of the correlation between soot and ice crystal numbers. This connection is integral for complete visions of the environmental implications of alternative aviation fuels. Precise data on contrail formation, containing the impact of biofuels, is crucial for climate models predicting the impact of aviation emissions on climate. The experimental establishment of the soot-ice crystal connection gives this understanding.

- *Properties of Soot Particle*: A study into the bimodal size distributions of soot particles in aircraft emissions is critical for focusing uncertainties on contrail formation and properties, with inferences for climate science and aviation practices. In-flight measurements uncover that freshly emitted soot particles usually exhibit a single peak in number-size distributions, but some cases play a second, larger particle mode in near-field contrails and dry plumes. The source of this larger mode remains uncertain, signifying that the bimodal distribution may survive in unrefined jet engine emissions rather than be caused by contrail processing or coagulation during plume development. Precise data on soot particle properties is essential for climate models incorporating contrail outcomes, and resolving the origin of bimodal size distributions is crucial to improving model representations of contrail properties. Policymakers and regulatory bodies rely on scientific research for progressing aviation-related environmental policies, making an understanding of soot particle size distributions significant for up-to-date decision-making.

- *Remote Sensing for Contrail-Cirrus*: Organized regional campaigns are important for estimating key variables in aging contrail-cirrus and aircraft plumes. This contains in-situ and remote sensing to portray the growth, decay, and trajectories of contrail ice particles, delivering essential data for interpretation of transformation and radiative effects. Estimation of contrail particles, ambient aerosols, and gaseous aerosol precursors notifies climate modeling and environmental assessments, connecting emissions to contrail properties. Gathered data validates climate models, enhancing their accuracy and improving the representation of contrail-cirrus effects. Understanding contrail-cirrus development supports in developing mitigation strategies, informing contrail avoidance, and reducing aviation's climate impact.

In addition to these research issues, there is a need to bridge the gaps with the assessment of the above-reported uncertainties and to investigate and improve the understanding of contrail avoidance and climate tradeoffs. Research should explore how to mitigate the climate impact of contrails without compromising aviation safety and efficiency.

7.3 Contrail avoidance and climate tradeoffs

To the best of our knowledge, no study has yet fully evaluated the contrail avoidance fuel and climate tradeoffs on a large scale, considering a sufficient number of routes and weather variation, while allowing full flight level optimization, quantifying the contrail impacts on an individual basis, and comparing to a fuel-optimal baseline in order to properly isolate the effects about contrail avoidance.

Gierens et al. (2008) proposed several potential ways to mitigate the impact of contrails, encompassing both technical and operational approaches. Regarding the technical aspect, they recognized the challenge of completely preventing contrail formation due to its primarily thermodynamic nature. However, they suggested the exploration of new engine cycles and

technical infrastructures that might help suppress contrails. Additionally, reducing the number of emitted particles was considered to mitigate contrail formation. While such evaluations would not eliminate contrails completely, they would produce thinner contrails with rarer but more ice crystals. These heavier ice crystals would incline more rapidly on average, causing shorter contrail lifetimes. The analysis also investigated operational mitigation options. Striking strict constraints, such as fixed maximum flight levels, was studied unreasonably due to the significant challenges it would pose for air traffic controllers and the resulting safety concerns. Their proposed strategies focused on addressing contrail formation both at the technical level through engine and infrastructure improvements and at the operational level by implementing flexible measures that consider real-time weather conditions. These approaches aimed to strike a balance between contrail reduction and the practical needs of aviation.

In a recent study, Sausen et al. (2023) presented an experiment that aimed to avoid contrail formation during real-world operations. This experiment took place in the Maastricht Upper Area Control region, covering parts of Germany, the Benelux countries, and the North Sea, in the year 2021. The researchers highlighted that contrail avoidance could serve as an effective method for mitigating the climate impact of aviation. To conduct their trial experiment, air traffic was deliberately diverted every other day by adjusting the flight altitude, either increasing or decreasing it by up to 2000 ft, whenever potential persistent contrails were predicted. The effectiveness of these deviations was assessed by analyzing satellite images of high clouds and employing a contrail detection algorithm that utilized contrail properties. Despite the ongoing challenge of accurately forecasting persistent contrails, the trial achieved a significant level of success, reaching 97.5%, suggesting that on average, persistent contrails can be avoided during regular flights in the real world through minor adjustments in the vertical flight path. Contrail avoidance through minor adjustments in flight paths represents a practical approach to mitigate the formation of persistent contrails. It demonstrates the feasibility of implementing such measures within air traffic management to reduce the environmental impact of aviation. The study highlights the potential for real-world applications of contrail avoidance as a means of addressing the climate effects of contrails. The findings of this experiment mark an important milestone in implementing operational measures in air traffic management to decrease the impact of climate from aviation.

In a recent Ph.D. thesis, Elmourad (2023) evaluated the fuel-climate tradeoffs arising from contrail avoidance strategies applied on a large scale. This study raises several key questions about contrails avoidance: What fraction of aviation's global total contrail length can be avoided using vertical re-routing exclusively? What is the fuel penalty of such an avoidance strategy? How does the fuel penalty or contrail reduction vary between flights or seasons? Can the fuel penalty be constrained? What effect does that have on the ability to do contrail avoidance? What net climate benefit can be achieved from contrail avoidance strategies? How does this differ from avoiding all contrails or only nighttime contrails? What are the relative orders of magnitude between the climate benefit from contrail avoidance and the climate damages from additional fuel burn? How does this difference compare with the uncertainties associated with contrail impacts?

As the global volume of air traffic continues to rise, the aviation industry grapples with a significant challenge in mitigating its environmental impact on climate change. Contrails, which contribute to global warming by trapping terrestrial radiation, have the potential to counteract the benefits of reduced emissions resulting from optimized flight paths. In a study by Roosenbrand et al. (2023), the authors conducted a global assessment of flights that contribute to contrail formation and assessed the altitude adjustments required to avoid these contrail-prone areas. This analysis

utilized a combination of data from the Integrated Global Radiosonde Archive (IGRA), which provides measurements from weather balloons with global coverage and high vertical resolution, and flight data from OpenSky. The study identified Mid-Western Europe, the Eastern United States of America, and Japan as regions characterized by both high air traffic volumes and a substantial percentage of flights forming contrails. Importantly, these regions offer opportunities for altitude adjustments of less than one kilometer to minimize contrail formation. The research also pinpointed other regions where relatively minor operational interventions could yield significant climate benefits.

Fuel-climate tradeoffs: While there have been numerous studies on operational contrail avoidance, there are still some research gaps in the field when it comes to understanding the fuel-climate tradeoffs that would follow a large-scale global application of contrail avoidance strategies.

Sustainable Aviation Fuel (SAF): Much still needs to be understood about what SAF will look like as it becomes the dominant fuel of the future. The emissions of soot and other particles from SAF are still not well understood and will have a significant effect on future contrail production and lifetimes. According to Bräuer et al. (2021,b), sustainable aviation fuels have been identified as capable of reducing both contrail ice numbers and the radiative forcing caused by contrail cirrus. Our study involved the measurement of apparent ice emission indices across different fuels with varying aromatic content at altitudes ranging from 9.1 to 9.8 km and 11.4 to 11.6 km. The data were collected during the ECLIF II/NDMAX flight experiment in January 2018, encompassing a variety of fuels differing in aromatic quantity and type. A comparison between a sustainable aviation fuel blend and a reference fuel Jet A-1 revealed a maximum reduction of 40% in apparent ice emission indices, highlighting the potential impact of sustainable aviation fuels on mitigating contrail-related environmental effects.

Alternative aircraft and new fuels: There is a lot of ongoing discussion about the potential development of aircraft using hydrogen as fuel. Such an aircraft engine would still emit water vapor and therefore could produce contrails. However, the major reduction in particulates, e.g., no soot, could affect the lifetime of the contrail and whether it could result in contrail cirrus. Research is needed to evaluate the potential for contrail production and resulting lifetimes. Other alternative fuels would also need to be evaluated.

Government research organizations and industry partners have an imperative to probe into the investigation and creation of sensor prototypes. One avenue of exploration is the development of a humidity sensor prototype with a precise range spanning from 20 parts per million by volume (ppmv) to well over 10,000 ppmv. The aim is to enhance the quality of measurements, particularly regarding temperature and relative humidity, at altitudes maintained during flight to address contrail mitigation. Equally, refining measurements at lower altitudes is crucial for enhancing weather forecasting accuracy. This accumulated data will play a pivotal role in evaluating and integrating these insights into forecast models, enhancing the robustness of these calculations. An additional area of focus is the refinement of model calculations pertaining to the impact of contrails, necessitating improved handling of variables such as clouds, aerosols, and specific aircraft characteristics.

8 Conclusions

This study reviews the current understanding of the impacts of contrail formation by aircraft on the Earth's climate system; it provides valuable insights into the current state of contrail research, offering perspectives on contrail formation, characteristics, life cycle, and potential future impacts.

1500 The study underscores the importance of confronting uncertainties in climate models and
1501 emphasizes the need for further research to enhance our understanding of contrail effects.

1502 Aviation emissions, encompassing both contrail cirrus clouds and carbon dioxide emissions, exert
1503 an important influence on the Earth's climate. Despite extensive research efforts, uncertainties
1504 persist, necessitating a deeper exploration of the microphysical processes governing contrail
1505 formation and aging. Our examination of global observational data and projections highlights the
1506 potential increase in contrail cirrus radiative forcing, as much a factor of three larger than the
1507 forcing from current emissions, by the mid-21st century, driven by many factors such as the
1508 likelihood for increased air traffic, potential enhancements in fuel efficiency, the introduction of
1509 alternative fuels, and the evolving atmospheric conditions. Addressing these complexities is
1510 imperative for the development of effective climate mitigation strategies and for identifying gaps
1511 in our knowledge.

1512

1513 **Author contributions.** DKS prepared the manuscript with support from SS and DJW

1514

1515 **Competing interests.** The author declares that they have no competing interests.

1516
1517 **Acknowledgment.**
1518 We thank Drs. Andrew Gettelman (Pacific Northwest National Laboratory, PNNL, USA), Ulrike
1519 Burkhardt (German Aerospace Center, DLR, Germany), Berndt Kärcher (DLR), Phillip J Ansell
1520 (University of Illinois at Urbana-Champaign, USA), D.S. Lee (Manchester Metropolitan
1521 University, UK), and Steven L Baughcum (The Boeing Company) for reviewing prior drafts of
1522 this report.

1523
1524 **Financial support**. The authors would like to thank the support from the Universities Space
1525 Research Association (USRA) through project subcontract 08600-031.

1526
1527
1528
1529
1530
1531 **References**
1532

1533 Airbus   Global   Market   Forecast: 2023-2042.   https://www.airbus.com/en/products
1534   services/commercial-aircraft/market/global-market-forecast, 2022.
1535 Appleman, H.: The formation of exhaust condensation trails by jet aircraft. Bull. Amer. Meteor.
1536   Soc., 34(1), 14-20, 1953.
1537 Atlas, D., Wang, Z., and Duda, D. P.: Contrails to cirrus: Morphology, microphysics, and radiative
1538   properties. J. Appl. Meteor., 45, 5–19, 2006.
1539 Aufm Kampe, H. J.: Die Physik der Auspuffwolken hinter Flugzeugen, Luftwissen, 10, 171–173,
1540   1943.
1541 Barrett, S., Prather, M., Penner, J., Selkirk, H., Balasubramanian, S., Dopelheuer, A., Fleming, G.,
1542   Gupta, M., Halthore, R., Hileman, J., Jacobson, M.: Guidance on the use of AEDT gridded
1543   aircraft emissions in atmospheric models. A technical note, Aug 17, 2010.

1544

1545   Baumgardner, D., Brenguier, J. L., Bucholtz, A., Coe, H., DeMott, P., Garrett, T. J., Gayet, J. F.,
1546   Hermann, M., Heymsfield, A., Korolev, A., Krämer, M.: Airborne instruments to measure
1547   atmospheric aerosol particles, clouds and radiation: A cook's tour of mature and emerging
1548   technology. Atmos. Res., 102(1-2), 10-29. Oct 1, 2011.
1549   Bier, A., and Burkhardt, U.: Variability in contrail ice nucleation and its dependence on soot
1550   number emissions. J. Geophys. Res. Atmos., 124(6), 3384–3400, 2019.
1551   Bier, A., and Burkhardt, U.: Impact of parametrizing microphysical processes in the jet and vortex
1552   phase on contrail cirrus properties and radiative forcing. J. Geophys. Res. Atmos., 127,
1553   e2022JD036677, 2022.
1554   Bier, A., Burkhardt, U., and Bock, L.: Synoptic control of contrail cirrus life cycles and their
1555   modification due to reduced soot number emissions. J. Geophys. Res. Atmos., 122(21),
1556   11,584–11,603, 2017.
1557   Bock, L., and Burkhardt, U.: Reassessing properties and radiative forcing of contrail cirrus using
1558   a global climate model. J. Geophys. Res. Atmos., 121(16), 9717–9736, 2016.
1559   Bock, L., and Burkhardt, U.: The temporal evolution of a long-lived contrail cirrus cluster:
1560   Simulations with a global climate model, J. Geophys. Res. Atmos., 121, 3548–3565, 2016.
1561   Bock, L., and Burkhardt, U.: Contrail cirrus radiative forcing for future air traffic. Atmos. Chem.
1562   Phys., 19(12), 8163–8174, 2019.
1563   Boeing: Commercial Market Outlook 2022–2041.
1564   https://www.boeing.com/commercial/market/commercial-market-outlook/index.page, 2022.
1565   Brasseur, G. P., Gupta, M., Anderson, B. E., Balasubramanian, S., Barrett, S., Duda, D., Fleming,
1566   G., Forster, P. M., Fuglestvedt, J., Gettelman, A., Halthore, R. N.: Impact of aviation on
1567   climate: FAA's aviation climate change research initiative (ACCRI) phase II, Bull. Amer.
1568   Meteor. Soc., 97(4), 561-583, Apr, 2016.
1569   Bräuer, T., Voigt, C., Sauer, D., Kaufmann, S., Hahn, V., Scheibe, M., Schlager, H., Diskin, G. S.,
1570   Nowak, J. B., DiGangi, J. P., Huber, F.: Airborne measurements of contrail ice properties-
1571   Dependence on temperature and humidity, Geophys. Res. Lett, 48(8), e2020GL092166, Apr
1572   28, (2021 a).
1573   Bräuer T, Voigt C, Sauer D, Kaufmann S, Hahn V, Scheibe M, Schlager H, Huber F, Le Clercq P,
1574   Moore RH, Anderson BE. Reduced ice number concentrations in contrails from low-aromatic
1575   biofuel blends. Atmospheric Chemistry and Physics. 21(22):16817-26., 2021 b
1576   Burkhardt, U., Kärcher, B., Ponater, M., Gierens, K., and Gettelman, A.: Contrail cirrus supporting
1577   areas in model and observations. Geophys. Res. Lett., 35, 2008.
1578   Burkhardt, U., and Kärcher, B.: Process-based simulation of contrail cirrus in a global climate
1579   model. J. Geophys. Res. Atmos., 114(D16), D16201, 2009.
1580   Burkhardt, U., Bock, L., and Bier, A.: Mitigating the contrail cirrus climate impact by reducing
1581   aircraft soot number emissions. npj Clim. Atmos. Sci., 1, 37, 2018.
1582   Burkhardt, U., and Kärcher, B.: Global radiative forcing from contrail cirrus. Nat. Clim. Change.,
1583   1, 54–58, 2011.
1584   Burkhardt, U., Kärcher, B., and Schumann, U.: Global modeling of the contrail and contrail cirrus
1585   climate impact. Bull. Am. Meteorol. Soc., 91(4), 479–484, 2010.
1586   Caiazzo, F., Agarwal, A., Speth, R. L., and Barrett, S. R. H.: Impact of biofuels on contrail
1587   warming. Environ. Res. Lett., 12, 114013, 2017.
1588   Carlin, B., Fu, Q., Lohmann, U., Mace, G., Sassen, K., and Comstock, J.: High-cloud horizontal
1589   inhomogeneity and solar albedo bias. J. Climate, 15, 2321–2339, 2002.

Chauvigné, A., Jourdan, O., Schwarzenboeck, A., Gourbeyre, C., Gayet, J. F., Voigt, C., Schlager, H., Kaufmann, S., Borrmann, S., Molleker, S., Minikin, A.: Statistical analysis of contrail to cirrus evolution during the Contrail and Cirrus Experiment (CONCERT). Atmos. Chem. Phys., 18(13), 9803-22, Jul 12, 2018.

Chen, C.-C., Gettelman, A., Craig, C., Minnis, P., and Duda, D.: Global contrail coverage simulated by CAM5 with the inventory of 2006 global aircraft emissions. J. Adv. Model. Earth Syst., 4(4), 2012.

Chen, C.-C., and Gettelman, A.: Simulated radiative forcing from contrails and contrail cirrus. Atmos. Chem. Phys. Discuss., 13, 10,939–10,959, 2013.

Chen, C.-C., and Gettelman, A.: Simulated 2050 Aviation Radiative Forcing from Contrails and Aerosols. Atmos. Chem. Phys., 16 (11), 7317–33, 2016.

Comstock, J. M., Ackerman, T. P., and Turner, D. D.: Evidence of high ice supersaturation in cirrus clouds using ARM Raman lidar measurements. Geophys. Res. Lett., 31, L11106, 2004.

Danabasoglu, G., Lamarque, J. F., Bacmeister, J., Bailey, D. A., DuVivier, A. K., Edwards, J., Emmons, L. K., Fasullo, J., Garcia, R., Gettelman, A., Hannay, C.: The community earth system model version 2 (CESM2). J. Adv. Model. Earth Syst., 12(2), e2019MS001916, Feb, 2020.

De Leon, R. R., M. Krämer, M., Lee, D. S., and Thelen, J. C.: Sensitivity of radiative properties of persistent contrails to the ice water path. Atmos. Chem. Phys., 12, 7893–7901, 2012.

Dietmüller, S., et al.: A new radiation infrastructure for the Modular Earth Submodel System (MESSy, based on version 2.51). Geosci. Model Dev., 9, 2209–2222, 2016.

Dipankar, A., Stevens, B., Heinze, R., Moseley, C., Zängl, G., Giorgetta, M., and Brdar, S.: Large eddy simulation using the general circulation model ICON. J. Adv. Model. Earth Syst., 7, 963–986, 2015.

Duda, D. P., Minnis, P., Nguyen, L., and Palikonda, R.: A case study of the development of contrail clusters over the Great Lakes. J. Atmos. Sci., 61, 1132–1146, 2004.

Duda, D. P., Minnis, P., Khlopenkov, K., Chee, T. L., and Boeke, R.: Estimation of 2006 Northern Hemisphere contrail coverage using MODIS data. Geophys. Res. Lett., 40, 612–617, 2013.

EASA (European Union Aviation Safety Agency) ICAO Aircraft Engine Emissions Databank 2023: http://www.easa.europa.eu/document-library/icao-aircraft-engine-emissions-databank.

Ettenreich, R.: Wolkenbildung über einer Feuersbrunst und an Flugzeugabgasen. Meteorol. Z., 36, 355–356, 1919.

Elmourad, J. A.: Evaluating Fuel-Climate Tradeoffs in Contrail Avoidance (Doctoral dissertation, Massachusetts Institute of Technology), 2023.

EUROCONTROL.: Aircraft Performance Summary Tables for the Base of Aircraft Date (BADA), 3.7, European Organisation for the Safety of Air Navigation, Brétigny-sur-Orge, 103, 2009.

Fritz, T. M., Eastham, S. D., Speth, R. L., and Barrett, S. R. H.: The role of plume-scale processes in long-term impacts of aircraft emissions. Atmos. Chem. Phys., https://doi.org/10.5194/acp-20-5697-2020, 2020.

Frömming, C., Ponater, M., Burkhardt, U., Stenke, A., Pechtl, S., and Sausen, R.: Sensitivity of contrail coverage and contrail radiative forcing to selected key parameters, Atmos. Environ., 45, 1483–1490, 2011.

Fuglestvedt, J. S., and coauthors: Transport impacts on atmosphere and climate: Metrics. Atmos. Environ, 44, 4648–4677, 2010.

Garber, D. P., Minnis, P., and Costulis, P. K.: A commercial flight track database for upper tropospheric aircraft emission studies over the USA and southern Canada, Meteorologische Zeitschrift, 14, 445–452, 2005.

Gayet, J. F., Shcherbakov, V., Voigt, C., Schumann, U., Schäuble, D., Jessberger, P., Petzold, A., Minikin, A., Schlager, H., Dubovik, O., Lapyonok, T.: The evolution of microphysical and optical properties of an A380 contrail in the vortex phase, Atmos. Chem. Phys., 12(14), 6629-6643, 2012.

Geleyn, J. F., Hollingsworth, A.: An economical analytical method for the computation of the interaction between scattering and line absorption of radiation, Beiträge zur Physik der Atmosphäre, 52, 1–16, 1978.

Gerz, T., Durbeck, T., Konopka, P.: Transport and effective diffusion of aircraft emissions, J. Geophys. Res., 103, 25905–25914, 1998.

Gettelman, A., Chen, C. C., Bardeen, C. G.: The climate impact of COVID-19-induced contrail changes, Atmos. Chem. Phys., 21(12), 9405-9416, 2021.

Gettelman, A., Chen, C.: The climate impact of aviation aerosols, Geophys. Res. Lett., 40(11), 2785-2789, 2013.

Gettelman, A., Morrison, H.: Advanced Two-Moment Bulk Microphysics for Global Models. Part I: Off-Line Tests and Comparison with Other Schemes, J. Climate, 28, 1268–1287, 2015.

Gettelman, A., Bardeen, C. G., McCluskey, C. S., Järvinen, E., Stith, J., Bretherton, C., McFarquhar, G., Twohy, C., D'Alessandro, J., Wu, W.: Simulating Observations of Southern Ocean Clouds and Implications for Climate, J. Geophys. Res., 125, 2020.

Gettelman, A., Gagne, D. J., Chen, C.-C., Christensen, M. W., Lebo, Z. J., Morrison, H., Gantos, G.: Machine Learning the Warm Rain Process, J. Adv. Model. Earth Syst., 13, 2021.

Gettelman, A., Hannay, C., Bacmeister, J. T., Neale, R. B., Pendergrass, A. G., Danabasoglu, G., Lamarque, J.-F., Fasullo, J. T., Bailey, D. A., Lawrence, D. M., Mills, M. J.: High Climate Sensitivity in the Community Earth System Model Version 2 (CESM2), Geophys. Res. Lett., 46, 8329–8337, 2019.

Gierens, K. M., Lim, L., Eleftheratos, K.: A review of various strategies for contrail avoidance, Open Atmos. Sci. J., 2, 1-7, 2008.

Gierens, K., Matthes, S., Rohs, S.: How Well Can Persistent Contrails Be Predicted?, Aerospace, 7, 169, 2020.

Gounou, A., Hogan, R. J.: A sensitivity study of the effect of horizontal photon transport on the radiative forcing of contrails, J. Atmos. Sci., 64, 1706–1716, 2007.

Graf, K., Schumann, U., Mannstein, H., Mayer, B.: Aviation induced diurnal North Atlantic cirrus cover cycle, Geophys. Res. Lett., 39, 2012.

Grewe, V., Gangoli Rao, A., Grönstedt, T., Xisto, C., Linke, F., Melkert, J., Middel, J., Ohlenforst, B., Blakey, S., Christie, S., Matthes, S., Dahlmann, K.: Evaluating the climate impact of aviation emission scenarios towards the Paris agreement including COVID-19 effects, Nat. Commun., 12, 3841, 2021.

Haywood, J. M., Allan, R. P., Bornemann, J., Forster, P. M., Francis, P. N., Milton, S., Rädel, G., Rap, A., Shine, K. P., Thorpe, R.: A case study of the radiative forcing of persistent contrails evolving into contrail-induced cirrus. J. Geophys. Res. Atmos., 114(D24), 2009.

ICAO Future Of Aviation 2012: https://www.icao.int/Meetings/FutureOfAviation/Pages/default.aspx, 2012

Immler, F., Treffeisen, R., Engelbart, D., Krüger, K., Schrems, O.: Cirrus contrails, and ice supersaturated regions in high-pressure systems at northern mid-latitudes, Atmos. Chem. Phys., 8, 1689–1699, 2008.

IPCC: Climate Change 2021: The Physical Science Basis. Contribution of Working Group I to the Sixth Assessment Report of the Intergovernmental Panel on Climate Change, 2021.

IPCC: Summary for Policymakers 2018: In V. Masson-Delmotte, P. Zhai, H. O. Pörtner, et al. (Eds.), Global warming of 1.5°C. An IPCC Special Report on the Impacts of Global Warming of 1.5°C above Pre-industrial Levels and Related Global Greenhouse Gas Emission Pathways, World Meteorological Organization Technical Document, pp. 32, 2018.

IPCC: Aviation and the global atmosphere 1999: In: Penner, J.E., Lister, D.H., Griggs, D. J., Dokken, D.J., McFarland, M. (Eds.), Intergovernmental Panel on Climate Change Special Report. Cambridge University Press, Cambridge, UK, 1999.

Irvine, E. A., Hoskins, B. J., Shine, K. P.: A Lagrangian analysis of ice-supersaturated air over the North Atlantic, J. Geophys. Res.: Atmospheres, 119, 90–100, 2013.

Jacobson, M. Z., Wilkerson, J. T., Naiman, A. D., Lele, S. K.: The effects of aircraft on climate and pollution. Part I: Numerical methods for treating the subgrid evolution of discrete size-and composition-resolved contrails from all commercial flights worldwide. J. Comput. Phys., 230(12), 5115-32, Jun 1, 2011.

Jacobson, M. Z.: Short-term effects of controlling fossil-fuel soot, biofuel soot and gases, and methane on climate, Arctic ice, and air pollution health. J. Geophys. Res., 115, D14209, 2010.

Jensen, E., Ackermann, A. S., Stevens, D. E., Toon, O. B., Minnis, P. Spreading and growth of contrails in a sheared environment. J. Geophys. Res., 103, 13557–13567, 1998.

Kärcher, B.: Formation and radiative forcing of contrail cirrus. Nat. Commun., 9, 1824, 2018.

Kärcher, B., Burkhardt, U., Bier, A., Bock, L., and Ford, I. J.: The microphysical pathway to contrail formation. J. Geophys. Res. Atmos., 120, 7893–7927, 2015.

Kärcher, B.: Formation and radiative forcing of contrail cirrus. Nat. Commun., 9(1), 1824, 2018.

Kärcher, B., and Yu, F.: Role of aircraft soot emissions in contrail formation. Geophys. Res. Lett., 36(1), L01804, 2009.

Kärcher, B., Burkhardt, U., Bier, A., Bock, L., and Ford, I. J.: The microphysical pathway to contrail formation. J. Geophys. Res. Atmos., 120(15), 7893–7927, 2015.

Klöwer, M., Allen, M. R., Lee, D. S., Proud, S. R., Gallagher, L., and Skowron, A.: Quantifying aviation's contribution to global warming. Environ. Res. Lett., 16, 104027, 2021.

Krämer, M., Rolf, C., Spelten, N., Afchine, A., Fahey, D., Jensen, E., Khaykin, S., Kuhn, T., Lawson, P., Lykov, A., Pan, L. L. (2020 Nov 2). A microphysics guide to cirrus–Part 2: Climatologies of clouds and humidity from observations. Atmospheric Chemistry and Physics, 20(21), 12569-608, 2020.

Krämer, M., Schiller, C., Afchine, A., Bauer, R., Gensch, I., Mangold, A., Schlicht, S., Spelten, N., Sitnikov, N., Borrmann, S., de Reus, M., and Spichtinger, P.: Ice supersaturations and cirrus cloud crystal numbers. Atmos. Chem. Phys., 9, 3505–3522, 2009.

Kristensson, A., Gayet, J.-F., Ström, J., and Auriol, F.: In situ observations of a reduction in effective crystal diameter in cirrus clouds near flight corridors. Geophys. Res. Lett., 27, 681–684, 2000.

Kübbeler, M., Hildebrandt, M., Meyer, J., Schiller, C., Hamburger, Th., Jurkat, T., Minikin, A., Petzold, A., Rautenhaus, M., Schlager, H., Schumann, U., Voigt, C., Spichtinger, P., Gayet, J.-F., Gourbeyre, C., and Krämer, M.: Thin and subvisible cirrus and contrails in a subsaturated environment. Atmos. Chem. Phys., 11, 5853–5865, 2011.

Kulik, L.: Satellite-based detection of contrails using deep learning. Master's thesis, Massachusetts Institute of Technology, 2019.

Kurz, C.: Entwicklung und Anwendung eines gekoppelten Klima-Chemie-Modellsystems: Globale Spurengastransporte und chemische Umwandlungsprozesse (Doctoral thesis). Ludwigs-Maximilians-University Munich, DLR Forschungsbericht, 2007.

Lamquin, N., Stubenrauch, C.J., Gierens, K., Burkhardt, U., and Smit, H.: A global climatology of upper tropospheric ice supersaturation occurrence inferred from the Atmospheric Infrared Sounder calibrated by MOZAIC. Atmos. Chem. Phys., 12, 381–405, 2012.

Lee, D. S., and Coauthors: Transport impacts on atmosphere and climate: Aviation. Atmos. Environ., 44, 4678–4734, 2010.

Lee, D. S., Fahey, D. W., Forster, P. M., Newton, P. J., Wit, R. C. N., Lim, L. L., Owen, B., and Sausen, R.: Aviation and global climate change in the 21st century. Atmos. Environ., 43, 3520-3537, https://doi.org/10.1016/j.atmosenv.2009.04.024, 2009.

Lee, D. S., Fahey, D. W., Skowron, A., Allen, M. R., Burkhardt, U., Chen, Q., Doherty, S. J., Freeman, S., Forster, P. M., Fuglestvedt, J., Gettelman, A., De León, R. R., Lim, L. L., Lund, M. T., Millar, R. J., Owen, B., Penner, J. E., Pitari, G., Prather, M. J., Sausen, R., and Wilcox, L. J.: The contribution of global aviation to anthropogenic climate forcing for 2000 to 2018. Atmos. Environ., 244, 117834, https://doi.org/10.1016/j.atmosenv.2020.117834, 2021.

Lewellen, D. C.: Analytic Solutions for Evolving Size Distributions of Spherical Crystals or Droplets Undergoing Diffusional Growth in Different Regimes. J. Atmos. Sci., 69, 417–434, 2012.

Lewellen, D. C.: Persistent contrails and contrail cirrus. Part II: Full lifetime behavior. J. Atmos. Sci., 71, 4420–4438, 2014.

Lewellen, D. C., Meza, O., Huebsch, W.: Persistent contrails and contrail cirrus. Part 1: Large-eddy simulations from inception to demise. J. Atmos. Sci., 71, 4399–4419, 2014.

Li, J., Caiazzo, F., Chen, N. Y., Sridhar, B., Ng, H., and Barrett, S.: Evaluation of aircraft contrails using dynamic dispersion model. AIAA Guidance Navigation, and Control (GNC) Conf., 2013–5178 pp., 2013.

Li, Y., Mahnke, C., Rohs, S., Bundke, U., Spelten, N., Dekoutsidis, G., Groß, S., Voigt, C., Schumann, U., Petzold, A., and Krämer, M.: Upper-tropospheric slightly ice-subsaturated regions: frequency of occurrence and statistical evidence for the appearance of contrail cirrus. Atmos. Chem. Phys., 23, 2251–2271, https://doi.org/10.5194/acp-23-2251-2023, 2023.

Liou, K.N., Takano, Y., Yue, Q., and Yang, P.: On the radiative forcing of contrail cirrus contaminated by black carbon. Geophys. Res. Lett., 40, 778–784, 2013.

Liu, X., Ma, P.-L., Wang, H., Tilmes, S., Singh, B., Easter, R. C., Ghan, S. J., and Rasch, P. J.: Description and evaluation of a new four-mode version of the Modal Aerosol Module (MAM4) within version 5.3 of the Community Atmosphere Model. Geosci. Model Dev., 9, 505–522, 2016.

Lohmann, U., Spichtinger, P., Heidt, S., Peter, T., and Smit, H.: Cirrus clouds and ice supersaturation regions in a global climate model. Environ. Res. Lett., 3(4), 045022, 2008.

Luebke, A. E., Afchine, A., Costa, A., Grooß, J.-U., Meyer, J., Rolf, C., Spelten, N., Avallone, L. M., Baumgardner, D., and Krämer, M.: The origin of midlatitude ice clouds and the resulting influence on their microphysical properties. Atmos. Chem. Phys., 16, 5793–5809, 2016.

Mannstein, H., Brömser, A., and Bugliaro, L.: Ground-based observations for the validation of contrails and cirrus detection in satellite imagery. Atmos. Meas. Tech., 3, 655–669, 2010.

Mannstein, H., Meyer, R., and Wendling, P.: Operational detection of contrails from NOAA-AVHRR data, Int. J. Remote Sens., 20, 1641–1660, 1999.

Markowicz, K. M., Witek, M. L.: Simulations of contrail optical properties and radiative forcing for various crystal shapes. J. Appl. Meteorol. Climatol., 50, 1740–1755, 1, 2011.

Marquart, S., Ponater, M., Mager, F., and Sausen, R.: Future Development of Contrail Cover, Optical Depth, and Radiative Forcing: Impacts of Increasing Air Traffic and Climate Change. J. Climate, 16, 2890–2904, 2, 2003.

Mayer, B., and Kylling, A.: The libRadtran software package for radiative transfer calculations: Description and examples of use. Atmos. Chem. Phys., 5, 1855–1877, https://doi.org/10.5194/acp-5-1855-2005, 2005.

McCloskey, K., Geraedts, S., Van Arsdale, C., and Brand, E.: A human-labeled landsat-8 contrails dataset. In ICML 2021 Workshop on Tackling Climate Change with Machine Learning, https://www.climatechange.ai/events/iclr2023#about, 2021.

Meerkötter, R., Schumann, U., Doelling, D. R., Minnis, P., Nakajima, T., and Tsushima, Y.: Radiative forcing by contrails. Ann. Geophys., 17, 1080–1094, https://doi.org/10.1007/s00585-999-1080-0, 1999.

Meijer, V. R., Kulik, L., Eastham, S. D., Allroggen, F., Speth, R. L., Karaman, S., and Barrett, S. R.: Contrail coverage over the United States before and during the COVID-19 pandemic. Environ. Res. Lett., 17, 034039, https://doi.org/10.1088/1748-9326/ac52f4, 2021.

Minnis, P.: Contrails. In G. R. North (Ed.), Encyclopedia of Atmospheric Sciences (2nd ed., Vol. 2, pp. 121-132). Oxford, UK: Elsevier Ltd., 2015.

Minnis, P., Bedka, S. T., Duda, D. P., Bedka, K. M., Chee, T., Ayers, J. K., Palikonda, R., Spangenberg, D. A., Khlopenkov, K. V., and Boeke, R.: Linear contrail and contrail cirrus properties determined from satellite data. Geophys. Res. Lett., 40, 3220–3226, https://doi.org/10.1002/grl.50557, 2013.

Minnis, P., Schumann, U., Doelling, D. R., Gierens, K. M., and Fahey, D. W.: Global distribution of contrail radiative forcing. Geophys. Res. Lett., 26, 1853–1856, 1999.

Molod, A., Takacs, L., Suarez, M., and Bacmeister, J.: Development of the GEOS-5 atmospheric general circulation model: evolution from MERRA to MERRA2. Geosci. Model Dev., 8, 1339–1356, 2015.

Myhre, G., and Stordal, F.: On the tradeoff of the solar and thermal infrared radiative impact of contrails. Geophys. Res. Lett., 28, 3119–3122, 2001.

Myhre, G., Kvalevåg, M., Rädel, G., Cook, J., Shine, K. P., Clark, H., Kärcher, F., Markowicz, K., Kardas, A., Wolkenberg, P., Balkanski, Y., Ponater, M., Forster, P., Rap, A., and De Leon, R. R.: Intercomparison of radiative forcing calculations of stratospheric water vapour and contrails. Meteorol. Z., 18, 585–596, 2009.

Naiman, A. D., Lele, S. K., Wilkerson, J. T., and Jacobson, M. Z.: Parameterization of subgrid plume dilution for use in large-scale atmospheric simulations. Atmos. Chem. Phys., 10, 2551–2560, 2009.

Naiman, A. D., Lele, S. K., Wilkerson, J. T., and Jacobson, M. Z.: A low order contrail model for use with global-scale climate models. 47th AIAA Aerospace Science Meeting, Orlando, FL, 2011.

Naiman, A. D., Lele, S. K., and Jacobson, M. Z.: Large Eddy simulations of persistent aircraft contrails. 49th AIAA Aerospace Science Meeting, Orlando, 2011.

Newinger, C., Burkhardt, U.: Sensitivity of contrail cirrus radiative forcing to air traffic scheduling. J. Geophys. Res. Atmos., 117, D1020, 2012.

1815 Neil Y. Chen, N., Sridhar, B., and Ng, H. K.: Prediction and use of contrail frequency index for
1816   contrail reduction strategies. AIAA Guidance, Navigation, and Control Conference, Toronto,
1817   Canada, 2010.
1818 Ng, J. Y. H., McCloskey, K., Cui, J., Brand, E., Sarna, A., Goyal, N., ... and Geraedts, S.:
1819   OpenContrails: Benchmarking Contrail Detection on GOES-16 ABI. arXiv preprint
1820   arXiv:2304.02122, 2023.
1821 Niklaß, M., Grewe, V., Gollnick, V., and Dahlmann, K.: Concept of climate-charged airspaces: a
1822   potential policy instrument for internalizing aviation's climate impact of non-CO2 effects.
1823   Climate Policy, 21, 1066–1085, 2021.
1824 Palikonda, R., Minnis, P., Duda, D. P., and Mannstein, H.: Contrail coverage derived from 2001
1825   AVHRR data over the continental United States of America and surrounding areas. Meteorol.
1826   Z., 14, 525–536, 2005.
1827 Paoli, R. and Shariff, K.: Contrail Modeling and Simulation. Annu. Rev. Fluid Mech., 48, 393–
1828   427, 2016.
1829 Penner, J. E., Lister, D. H., Griggs, D. J., Dokken, D. J., and McFarland, M., Eds.: Aviation and
1830   the Global Atmosphere. Cambridge University Press, 373 pp., 1999.
1831 Petters, M. D., and Kreidenweis, S. M.: A single parameter representation of hygroscopic growth
1832   and cloud condensation nucleus activity. Atmos. Chem. Phys., 7(8), 1961–1971, 2007.
1833 Petzold, A., Busen, R., Schröder, F. P., Baumann, R., Kuhn, M., Ström, J., Hagen, D. E.,
1834   Whitefield, P. D., Baumgardner, D., Arnold, F., Borrmann, S., and Schumann, U.: Near-field
1835   measurements on contrail properties from fuels with different sulfur content. J. Geophys. Res.
1836   Atmos., 102, 29867–29880, 1997.
1837 Petzold, A., Krämer, M., Neis, P., Rolf, C., Rohs, S., Berkes, F., Smit, H. G. J., Gallagher, M.,
1838   Beswick, K., Lloyd, G., Baumgardner, D., Spichtinger, P., Nédélec, P., Ebert, V., Buchholz,
1839   B., Riese, M., and Wahner, A.: Upper tropospheric water vapor and its interaction with cirrus
1840   clouds as seen from IAGOS long-term routine in situ observations. Faraday Discuss, 200, 229–
1841   249, 2017.
1842 Poellot, M. R., Arnott, W. P., and Hallett, J.: In situ observations of contrail microphysics and
1843   implications for their radiative impact. J. Geophys. Res., 104, 12 077–12 084, 1999.
1844 Pomroy, H.R., and Illingworth, J.A.: Ice cloud inhomogeneity: quantifying bias in emissivity from
1845   radar observations. Geophys. Res. Lett., 27, 2101–2104, 2000.
1846 Ponater, M., Marquart, S., and Sausen, R.: Contrails in a comprehensive global climate model:
1847   Parameterization and radiative forcing results. J. Geophys. Res. Atmos., 107, ACL 2-1–ACL
1848   2-15, 2002.
1849 Pruppacher, H. R. and Klett, J. D.: Microphysics of Clouds and Precipitation, Atmospheric and
1850   Oceanographic Sciences Library, 2nd Edn., Kluwer Academic Publishers, Dordrecht, the
1851   Netherlands, ISBN 978-0792344094, 1997.
1852 Pruppacher, H. R. and Klett, J. D.: Microphysics of clouds and precipitation, Kluwer Academic,
1853   Norwell, Mass., 2000.
1854 Rädel, G. and Shine, K. P.: Radiative forcing by persistent contrails and its dependence on cruise
1855   altitudes. J. Geophys. Res. Atmos., 113, D07105, 2008.
1856 Rap, A., Forster, P. M., Jones, A., Boucher, O., Haywood, J. M., Bellouin, N., and De Leon, R.
1857   R.: Parameterization of contrails in the UK Met Office Climate Model. J. Geophys. Res., 115,
1858   D10205, 2010.
1859 Righi, M., Hendricks, J., and Sausen, R.: The global impact of the transport sectors on atmospheric
1860   aerosol: simulations for year 2000 emissions. Atmos. Chem. Phys., 13, 9939–9970, 2013.

1861 Righi M, Hendricks J, Beer CG. Exploring the uncertainties in the aviation soot–cirrus effect.
1862   Atmos. Chem. Phys. Nov 30;21(23):17267-89, 2021
1863 Roeckner, E., Baeuml, G., Bonventura, L., Brokopf, R., Esch, M., Giorgetta, M., Hagemann, S.,
1864   Kirchner, I., Kornblueh, L., Manzini, E., Rhodin, A., Schlese, U., Schulzweida, U., and
1865   Tompkins, A.: The atmospheric general circulation model ECHAM5. PART I Model
1866   description, Report 349. Max Planck Institute for Meteorology, Hamburg, Germany.
1867 Roosenbrand E, Sun J, Hoekstra J. Optimizing Global Flight Altitudes for Contrail
1868   Reduction. Insights from Open Flight and Weather Balloon Data. Fifteenth USA/Europe Air
1869   Traffic Management Research and Development Seminar (ATM2023)
1870 Sanz-Morère, I., Eastham, S. D., Allroggen, F., Speth, R. L., and Barrett, S. R. H: Impacts of multi-
1871   layer overlap on contrail radiative forcing. Atmos. Chem. Phys., 21, 1649–1681, 2021.
1872 Sausen, R., K. Gierens, M. Ponater, and U. Schumann: A diagnostic study of the global distribution
1873   of contrails. Part I: Present-day climate. Theoretical and Applied Climatology, 61, 127–141,
1874   1998.
1875 Sausen, R., Hofer, S. M., Gierens, K. M., Bugliaro Goggia, L., Ehrmanntraut, R., Sitova, I., ... and
1876   Miller, N.: Can we successfully avoid persistent contrails by small altitude adjustments of
1877   flights in the real world?. Meteorologische Zeitschrift, 2023.
1878 Schmidt, E: Die Entstehung von Eisnebel aus den Auspuffgasen von Flugmotoren, in: Schriften
1879   der Deutschen Akademie der Luftfahrtforschung, Verlag R. Oldenbourg, München, Heft 44,1–
1880   15, 1941.
1881 Schröder, F., Kärcher, B., Duroure, C., Ström, J., Petzold, A., Gayet, J.-F., Strauss, B., Wendling,
1882   P., and Borrmann, S.: On the Transition of Contrails into Cirrus Clouds. J. Atmos. Sci., 57,
1883   464–480, 2000.
1884 Schumann, U., and Graf, K.: Aviation-induced cirrus and radiation changes at diurnal timescales.
1885   J. Geophys. Res., 118, 2404–2421, 2013.
1886 Schumann, U., and Heymsfield, A.: On the lifecycle of individual contrails and contrail cirrus-Ice
1887   Formation and Evolution in Clouds and Precipitation: Measurement and Modeling Challenges:
1888   Chapter 3, Meteor. Monogr, 3.1–3.24, 2016.
1889 Schumann, U., and Wendling, P.: Determination of contrails from satellite data and observational
1890   results. Air Traffic and the Environment-Background, Tendencies and Potential Global
1891   Atmospheric Effects, U. Schumann, Ed., Lecture Notes in Engineering, Springer-Verlag, 138–
1892   153, 1990.
1893 Schumann, U., Baumann, R., Baumgardner, D., Bedka, S. T., Duda, D. P., Freudenthaler, V.,
1894   Gayet, J.-F., Heymsfield, A. J., Minnis, P., Quante, M., Raschke, E., Schlager, H., Vázquez-
1895   Navarro, M., Voigt, C., and Wang, Z.: Properties of individual contrails: a compilation of
1896   observations and some comparisons. Atmos. Chem. Phys., 17, 403–438, 2017.
1897 Schumann, U., Bugliaro, L., Dörnbrack, A., Baumann, R., and Voigt, C.: Aviation Contrail Cirrus
1898   and Radiative Forcing Over Europe During 6 Months of COVID-19. Geophys. Res. Lett., 48,
1899   2021.
1900 Schumann, U., Penner, J.E., Chen, Y., Zhou, C., and Graf, K.: Dehydration effects from contrails
1901   in a coupled contrail-climate model. Atmos. Chem. Phys., 15, 11179-11199, 2015.
1902 Schumann, U., Ström, J., Busen, R., Baumann, R., Gierens, K., Krautstrunk, M., Schröder, F. P.,
1903   and Stingl, J.: In situ observations of particles in jet aircraft exhausts and contrails for different
1904   sulfur-containing fuels. J. Geophys. Res., 101, 6853–6870, 1996.
1905 Schumann, U.: A contrail cirrus prediction model. Geosci. Model Dev., 5, 543-580, 2012.

Schumann, U.: On conditions for contrail formation from aircraft exhausts. Meteorol. Z., 5, 4-23, 1996.

Schumann, U., Konopka, P., Baumann, R., Busen, B., Gerz, T., Schlager, H., Schulte, P., and Volkert, H.: Estimate of diffusion parameters of aircraft exhaust plumes near the tropopause from nitric oxide and turbulence measurements. J. Geophys. Res., 100, 147-162, 1995.

Siddiqui, N: Atmospheric Contrail Detection with a Deep Learning Algorithm, Scholarly Horizons: Univ. Minnesota Morris Undergraduate Journal, Vol. 7: Iss. 1, Article 5, 2020.

Spangenberg, D. A., Minnis, P., Bedka, S. T., Palikonda, R., Duda, D. P., and Rose, F. G.: Contrail radiative forcing over the Northern Hemisphere from 2006 Aqua MODIS data. Geophys. Res. Lett., 40, 595–600, 2013.

S Spinhirne, J. D., Hart, W. D., and Duda, D. P.: Evolution of the morphology and microphysics of contrail cirrus from airborne remote sensing. Geophys. Res. Lett., 25, 1153–1156, doi:10.1029/97GL03477, 1998.

Sridhar, B., Ng, H. K., and Chen, N. Y.: Aircraft Trajectory Optimization and Contrails Avoidance in the Presence of Winds, 10th AIAA Aviation Technology, Integration and Operations Conference (ATIO), Fort Worth, TX, 2010.

Stier, P., Feichter, J., Kinne, S., Kloster, S., Vignati, E., Wilson, J., et al.: The aerosol-climate model ECHAM5-HAM. Atmos. Chem. Phys., 5(4), 1125–1156, 2005.

Stocker, T.F., Qin, D., Plattner, G.K., Tignor, M., Allen, S.K., Boschung, J., Nauels, A., Xia, Y., Bex, V., Midgley, P. M. (Eds.): Climate Change 2013: the Physical Science Basis, Contribution of Working Group I to the Fifth Assessment Report of the Intergovernmental Panel on Climate Change. Cambridge University Press, Cambridge, United Kingdom and New York, NY, USA, 2013.

Stuber, N., Sausen, R., and Ponater, M.: Stratosphere adjusted radiative forcing calculations in a comprehensive climate model. Theor. Appl. Climatol., 68(3–4), 125–135, 2001.

Sun J, Roosenbrand E. Flight Contrail Segmentation via Augmented Transfer Learning with Novel SR Loss Function in Hough Space. arXiv preprint arXiv:2307.12032. 2023 Jul 22.

Taylor, K. E., Williamson, D., and Zwiers, F.: The sea surface temperature and sea-ice concentration boundary conditions for AMIP II simulations, PCMDI report no. 60, program for climate model diagnostics and intercomparison. The University of California, Lawrence Livermore National Laboratory, 2000.

Tesche, M., Achtert, P., Glantz, P., and Noone, K. J.: Aviation effects on already-existing cirrus clouds. Nat. Commun., 7(1), 12016, 2016.

Unterstrasser, S.: Properties of young contrails-A parametrization based on large-eddy simulations. Atmos. Chem. Phys., 16(4), 2059–2082, 2016.

Unterstrasser, S., and Sölch, I.: Numerical modeling of contrail cluster formation. Proc. Third Int. Conf. on Transport, Atmosphere and Climate (TAC-3). Prien am Chiemsee, Germany, DLR, 114–119, 2012.

Unterstrasser, S., and Görsch, N.: Aircraft-type dependency of contrail evolution. J. Geophys. Res.-Atmos., 119, 14 015–14 027, 2014.

Unterstrasser, S., Gierens, K., Sölch, I., and Wirth, M.: Numerical simulations of homogeneously nucleated natural cirrus and contrail-cirrus. Part 2: Interaction on a local scale. Meteorol. Z., 26, 643–661, 2017.

Vazquez-Navarro, M., Mannstein, H., and Kox, S.: Contrail life cycle and properties from 1 year of msg/seviri rapid scan images. Atmos. Chem. Phys., 15 (15):8739–8749, 2015.

Vázquez-Navarro, M., Mannstein, H., and Mayer, B.: An automatic contrail tracking algorithm. Atmos. Meas. Tech., 3, 1089–1101, 2010.

1953 Vazquez-Navarro, M., Mayer, B., and Mannstein, H.: A fast method for the retrieval of integrated
1954   longwave and shortwave top-of-atmosphere upwelling irradiances from msg/severe (drums).
1955   Atmos. Meas. Tech., 6(10):2627–2640, 2013.
1956 Verma, P., and Burkhardt, U.: Contrail formation within cirrus: ICON-LEM simulations of the impact
1957   of cirrus cloud properties on contrail formation. Atmos. Chem. Phys., 22(13), 8819-8842, 2022.
1958 Voigt, C., Schumann, U., Jessberger, P., Jurkat, T., Petzold, A., Gayet, J.-F., Krämer, M., Thornberry,
1959   T., and Fahey, D. W: Extinction and optical depth of contrails. Geophys. Res. Lett., 38, L11806,
1960   2011.
1961 Voigt, C., Schumann, U., Jurkat, T., Schäuble, D., Schlager, H., Petzold, A., Gayet, J.-F., Krämer, M.,
1962   Schneider, J., Borrmann, S., Schmale, J., Jessberger, P., Hamburger, T., Lichtenstern, M., Scheibe,
1963   M., Gourbeyre, C., Meyer, J., Kübbeler, M., Frey, W., Kalesse, H., Butler, T., Lawrence, M. G.,
1964   Holzäpfel, F., Arnold, F., Wendisch, M., Döpelheuer, A., Gottschaldt, K., Baumann, R., Zöger,
1965   M., Sölch, I., Rautenhaus, M., and Dörnbrack, A: In-situ observations of young contrails– overview
1966   and selected results from the CONCERT campaign. Atmos. Chem. Phys., 10, 9039– 9056, 2010.
1967 Voigt, C., Schumann, U., Minikin, A., Abdelmonem, A., Afchine, A., Borrmann, S., Boettcher, M.,
1968   Buchholz, B., Bugliaro, L., Costa, A., Curtius, J.: ML-CIRRUS: The airborne experiment on
1969   natural cirrus and contrail cirrus with the high-altitude long-range research aircraft HALO. B. Am.
1970   Meteorol. Soc., 98, 271–288, 2017.
1971 Weickmann, H.: Formen und Bildung atmosphärischer Eiskristalle. Beitr. Phys. freien Atmos., 28, 33,
1972   1945.
1973 Wilkerson, J. T., Jacobson, M. Z., Malwitz, A., Balasubramanian, S., Wayson, R., Fleming, G., et al.:
1974   Analysis of emission data from global commercial aviation: 2004 and 2006. Atmos. Chem. Phys.,
1975   10(13), 6391–6408, 2010.
1976 Wolf K, Bellouin N, Boucher O. Sensitivity of cirrus and contrail radiative effect on cloud
1977   microphysical and environmental parameters. Atmos. Chem. Phys. 9;23(21):14003-37, 2023.
1978 Wuebbles, D., Gupta, M., and Ko, M.: Evaluating the impacts of aviation on climate change. Eos,
1979   Trans. AGU, 88(14), 157-160, 2007.
1980 Wuebbles, D., Forster, P., Rogers, H., and Herman, R.: Issues and uncertainties affecting metrics for
1981   aviation impacts on climate. Bull. Amer. Meteor. Soc., 91(4), 491-496, 2010.
1982 Xie, Y., Yang, P., Liou, K.N., Minnis, P., and Duda, D. P.: Parameterization of contrail radiative
1983   properties for climate studies. Geophys. Res. Lett., 39, L00F02, 2012.
1984 Yi, B., Yang, P., Liou, K.N., Minnis, P., and Penner, J. E.: Simulation of the global contrail radiative
1985   forcing: A sensitivity analysis. Geophys. Res. Lett., 39, L00F03, 2012.
1986 Yun, Y., Penner, J. E., and Popovicheva, O.: The effects of hygroscopicity on ice nucleation of fossil
1987   fuel combustion aerosols in mixed-phase clouds. Atmos. Chem. Phys., 13, 4339–4348, 2013.
1988 Zängl, G., Reinert, D., Rípodas, P., and Baldauf, M.: The ICON (ICOsahedral Non-hydrostatic)
1989   modelling framework of DWD and MPI-M: Description of the non-hydrostatic dynamical core. Q.
1990   J. R. Meteorol. Soc., 141(687), 563-579, 2015.
1991 Zhou, C., and Penner, J. E.: Aircraft soot indirect effect on large-scale cirrus clouds: Is the indirect
1992   forcing by aircraft soot positive or negative? J. Geophys. Res.: Atmos., 119, 11 303–11 320, 2014.